Gastroenterology 2021;161:1584–1600

BASIC AND TRANSLATIONAL—PANCREAS

Metabolic Rewiring by Loss of Sirt5 Promotes Kras-Induced Pancreatic Cancer Progression

Tuo Hu,[1,2] Surendra K. Shukla,[1] Enza Vernucci,[1] Chunbo He,[1] Dezhen Wang,[1] Ryan J. King,[1] Kanupriya Jha,[3] Kasturi Siddhanta,[1,4] Nicholas J. Mullen,[1] Kuldeep S. Attri,[1] Divya Murthy,[1] Nina V. Chaika,[1] Ravi Thakur,[1] Scott E. Mulder,[1,4] Camila G. Pacheco,[1] Xiao Fu,[1] Robin R. High,[5] Fang Yu,[5] Audrey Lazenby,[6] Clemens Steegborn,[7] Ping Lan,[2] Kamiya Mehla,[1] Dante Rotili,[8] Sarika Chaudhary,[3] Sergio Valente,[8] Marco Tafani,[9] Antonello Mai,[8] Johan Auwerx,[10] Eric Verdin,[11] David Tuveson,[12] and Pankaj K. Singh[1,4,6,13]

[1]The Eppley Institute for Research in Cancer and Allied Diseases, University of Nebraska Medical Center, Omaha, Nebraska; [2]Department of Colorectal Surgery, Guangdong Provincial Key Laboratory of Colorectal and Pelvic Floor Diseases, The Sixth Affiliated Hospital, Sun Yat-sen University, Guangzhou, Guangdong, China; [3]Department of Biotechnology, School of Engineering and Applied Sciences, Bennett University, Greater Noida, Uttar Pradesh, India; [4]Department of Biochemistry and Molecular Biology, University of Nebraska Medical Center, Omaha, Nebraska; [5]Department of Biostatistics, University of Nebraska Medical Center, Omaha, Nebraska; [6]Department of Pathology and Microbiology, University of Nebraska Medical Center, Omaha, Nebraska; [7]University of Bayreuth, Department of Biochemistry, Bayreuth, Germany; [8]Department of Drug Chemistry and Technologies, Sapienza University of Rome, Rome, Italy; [9]Department of Experimental Medicine, Sapienza University of Rome, Rome, Italy; [10]Laboratory for Integrative Systems Physiology, Ecole Polytechnique Fédérale de Lausanne, Lausanne, Switzerland; [11]Buck Institute for Research on Aging, Novato, California; [12]Cancer Center at Cold Spring Harbor Laboratory, Cold Spring Harbor, New York; and [13]Fred & Pamela Buffett Cancer Center, University of Nebraska Medical Center, Omaha, Nebraska

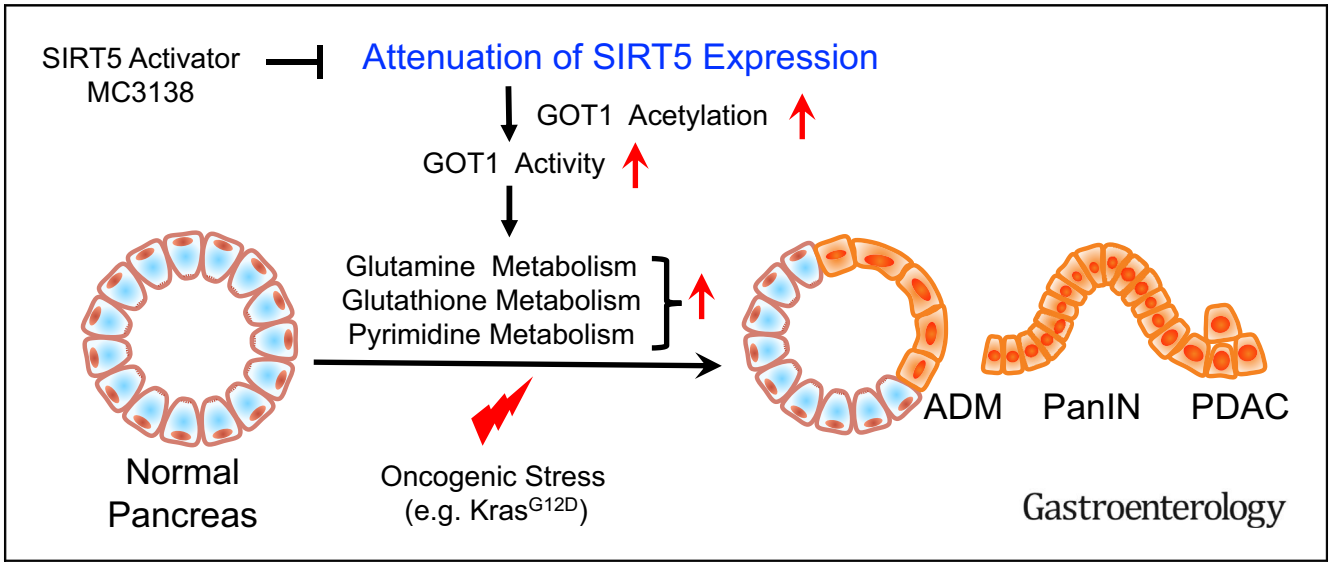

See Covering the Cover synopsis on page 1352; See editorial on page 1376.

BACKGROUND & AIMS: SIRT5 plays pleiotropic roles via post-translational modifications, serving as a tumor suppressor, or an oncogene, in different tumors. However, the role SIRT5 plays in the initiation and progression of pancreatic ductal adenocarcinoma (PDAC) remains unknown. **METHODS:** Published datasets and tissue arrays with SIRT5 staining were used to investigate the clinical relevance of SIRT5 in PDAC. Furthermore, to define the role of SIRT5 in the carcinogenesis of PDAC, we generated autochthonous mouse models with conditional *Sirt5* knockout. Moreover, to examine the mechanistic role of SIRT5 in PDAC carcinogenesis, SIRT5 was knocked down in PDAC cell lines and organoids, followed by metabolomics and proteomics studies. A novel SIRT5 activator was used for therapeutic studies in organoids and patient-derived xenografts. **RESULTS:** SIRT5 expression negatively regulated tumor cell proliferation and correlated with a favorable prognosis in patients with PDAC. Genetic ablation of *Sirt5* in PDAC mouse models promoted acinar-to-ductal metaplasia, precursor lesions, and pancreatic tumorigenesis, resulting in poor survival. Mechanistically, SIRT5 loss enhanced glutamine and glutathione metabolism via acetylation-mediated activation of GOT1. A selective SIRT5 activator, MC3138, phenocopied the effects of

SIRT5 overexpression and exhibited antitumor effects on human PDAC cells. MC3138 also diminished nucleotide pools, sensitizing human PDAC cell lines, organoids, and patient-derived xenografts to gemcitabine. **CONCLUSIONS:** Collectively, we identify SIRT5 as a key tumor suppressor in PDAC, whose loss promotes tumorigenesis through increased noncanonic use of glutamine via GOT1, and that SIRT5 activation is a novel therapeutic strategy to target PDAC.

Keywords: SIRT5; GOT1; Pancreatic Cancer; Glutamine Metabolism; Glutathione Metabolism.

WHAT YOU NEED TO KNOW

BACKGROUND AND CONTEXT

Pancreatic ductal adenocarcinoma (PDAC) cells with activating *KRAS* mutations use glutamine in a noncanonic way via the GOT2-GOT1-ME1 pathway. SIRT5 has pleiotropic roles, serving as an oncogene and tumor suppressor in different cancers.

NEW FINDINGS

SIRT5 is a novel tumor suppressor for pancreatic cancer and genetically targeting SIRT5 makes PDAC tumors more aggressive. SIRT5 negatively regulates noncanonic glutamine metabolism via direct post-translational modifications of GOT1. Activation of SIRT5 with a novel small molecule is a potential new therapy for PDAC with low-SIRT5 levels.

LIMITATIONS

This study was conducted in PDAC cell lines, genetically engineered mice models, and human tissue samples (tissue microarrays, PDAC organoids, and patient-derived xenografts). More work needs to be done in human patients.

IMPACT

SIRT5 activation (small-molecule SIRT5-activator MC3138) combined with gemcitabine may lead to a novel safe and effective therapy for patients with PDAC with low–tumoral SIRT5 expression.

A remarkable feature of pancreatic ductal adenocarcinoma (PDAC) is the hypoxic, harsh, and nutrient-deficient tumor microenvironment.[1] Accordingly, PDAC cells tend to reprogram their metabolic pathways to survive and grow under these harsh conditions.[1–3] Therefore, a deeper understanding of the biological features and molecular regulation of metabolic dependencies of PDAC is strongly expected to provide novel targets for therapeutic interventions.

Unlike many other cells using glutamine to feed the tricarboxylic acid cycle via glutamate dehydrogenase 1 (GLUD1), PDAC cells metabolize glutamine in a noncanonic way.[4,5] Mitochondrial aspartate aminotransferase (glutamate-oxaloacetate transaminase 2 [GOT2]) converts glutamine to aspartate (Asp). Glutamine-derived Asp is transported to the cytoplasm. Next, cytosolic Asp aminotransferase (GOT1) converts glutamine-derived Asp to oxaloacetate, which is converted to malate by cytosolic malate dehydrogenase. Then, the cytoplasmic malic enzyme 1 (ME1) catalyzes the oxidative decarboxylation of malate to pyruvate, with a concomitant production of reduced nicotinamide adenine dinucleotide phosphate (NADPH), sustaining the redox homeostasis in PDAC cells. This noncanonic glutamine metabolic pathway is dispensable in normal cells, but it has the potential to serve as a promising therapeutic target in PDAC.

Sirtuins (SIRT1–SIRT7) are a class of evolutionarily conserved nicotinamide adenine dinucleotide (NAD^+)–dependent enzymes that possess deacetylase, desuccinylase, deglutarylase, and demalonylase activity.[6,7] Sirtuins have been implicated in cancer progression due to their roles in regulating cancer cell metabolism, tumor microenvironment, and genome stability.[8] Among the 7 mammalian sirtuins, SIRT5 has been shown to be located in both the mitochondria and the cytosol.[9–11] Given the pleiotropic role of SIRT5 in regulating cancer cell metabolism, it potentially can act as a tumor suppressor, or in contrast as an oncogene, in different cancer types and microenvironments by mediating the post-translational modification of its target substrates.[12–19] Yet, the function of SIRT5 in the initiation and progression of PDAC remains obscure.

The present study revealed SIRT5 to be down-regulated in both human PDAC tissues and murine pancreatic tumors. Furthermore, we found SIRT5 deletion to accelerate tumor growth and to correlate with poor survival in both patients with PDAC and genetically engineered mouse models. By integrating mass spectrometry–based metabolomics and proteomics with biochemical assays, GOT1 was identified as the critical target substrate in SIRT5-regulated PDAC progression. Mechanistically, SIRT5 deletion enhanced the enzyme activity of GOT1 by facilitating GOT1 acetylation. Importantly, SIRT5 activation with a novel small-molecule activator MC3138 inhibited proliferation in SIRT5-low PDAC cell lines and organoids. Furthermore, SIRT5 activation decreased nucleotide levels and facilitated synergy with gemcitabine in human PDAC organoids and patient-derived xenografts (PDX). Thus, the present study demonstrates SIRT5 activation, in combination with gemcitabine, as a potential therapeutic strategy in PDAC.

Materials and Methods

Cell Culture

Human PDAC cell lines Capan1, Capan2, AsPC1, PANC-1, CFPAC-1, SW1990, and MIAPaCa-2, and HEK 293T were obtained from the American type culture collection (ATCC,

Abbreviations used in this paper: **AOA, aminooxyacetate; Asp, aspartate; CS, *Pdx1-Cre, Sirt5*$^{fl/fl}$; GLUD1, glutamate dehydrogenase 1; GOT, glutamate-oxaloacetate transaminase; GSH, glutathione; IC50, half maximal inhibitory concentration; KCS, *Pdx1-Cre, LSL-Kras*^{G12D}, *Sirt5*$^{fl/fl}$; KPC, *Kras*$^{G12D/+}$, *p53*$^{R172H/+}$, *Pdx1-Cre*$^{tg/+}$; KPCS, *Pdx1-Cre, LSL-Kras*^{G12D}, *LSL-Tp53*^{R172H}, *Sirt5*$^{fl/fl}$; ME1, malic enzyme 1; mRNA, messenger RNA; NAD, nicotinamide adenine dinucleotide; NADPH, reduced nicotinamide adenine dinucleotide phosphate; PanIN, pancreatic intraepithelial neoplasia; PCR, polymerase chain reaction; PDAC, pancreatic ductal adenocarcinoma; PDX, patient-derived xenografts; SIRT, sirtuin; UNMC, University of Nebraska Medical Center.**

Most current article

0016-5085
https://doi.org/10.1053/j.gastro.2021.06.045

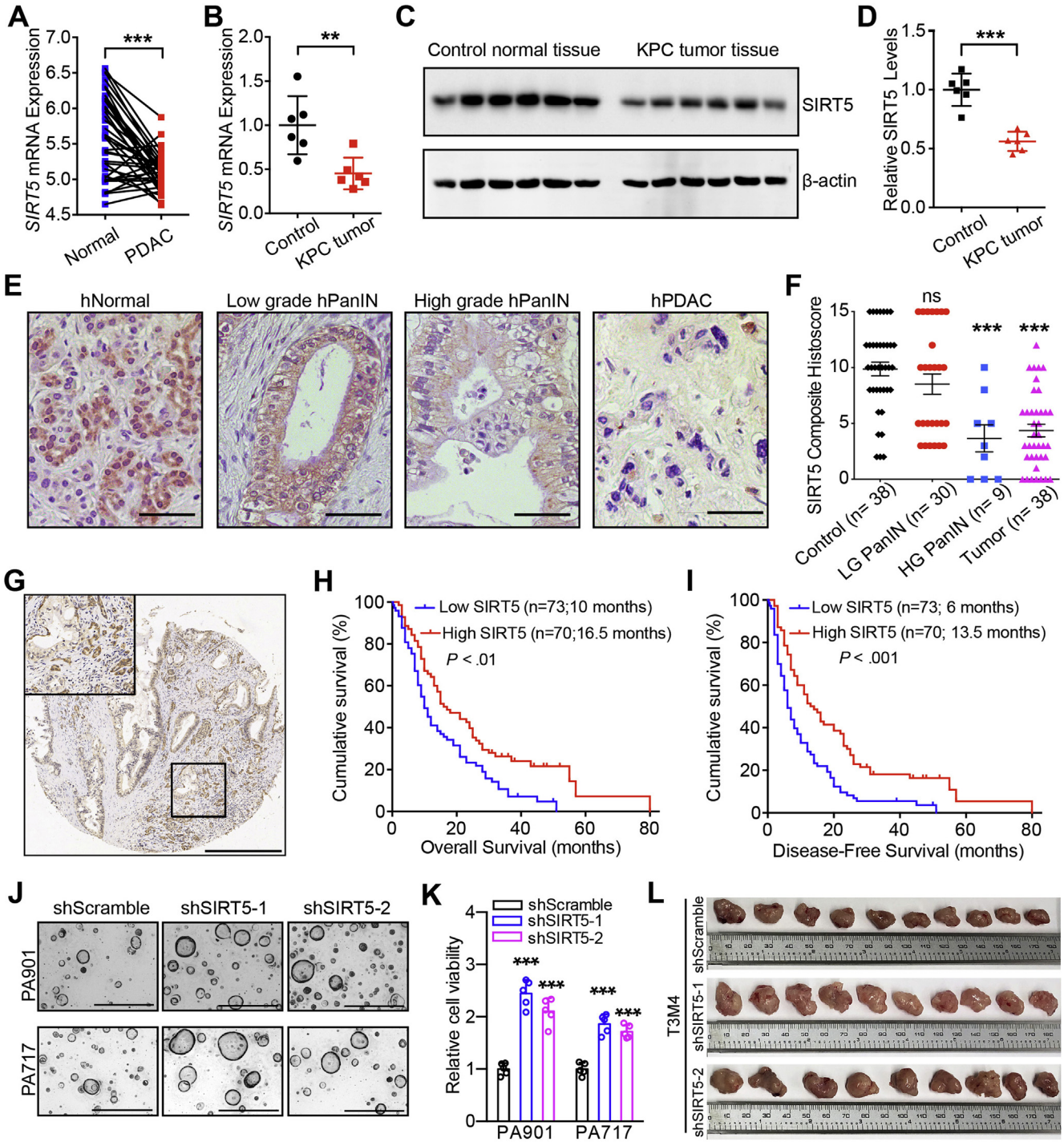

Figure 1. SIRT5 down-regulation in PDAC correlates with disease progression, poor survival outcomes, and enhanced tumor cell growth. (A) SIRT5 mRNA levels in pancreatic cancer tissues and the paired adjacent normal tissues (39 pairs) from GEO database. (*B–D*) *Sirt5* mRNA (B) and protein (*C–D*) levels in 25-week-old Cre control and KPC pancreatic cancer tissues. (*E–F*) Immunohistochemistry (IHC) staining and quantification for SIRT5 expression in adjacent normal tissues, low-grade and high-grade PanINs, and pancreatic tumors. Scale bar 100 μm. (G) Representative IHC staining for SIRT5 expression in pancreatic cancer tissue microarrays. Scale bar 500 μm. (*H–I*) Survival analysis of patients with pancreatic cancer categorized by low- and high-SIRT5 expression. (*J–K*) Representative images and cell viability for control and *SIRT5*-knockdown organoids cultured for 7 days. Scale bar 1000 μm. (*L–N*) Representative image, tumor volume (mean ± SE) and tumor weight of control and *SIRT5*-knockdown tumors. (*O–P*) Ki67 staining and quantitation in control and *SIRT5*-knockdown tumors. Scale bar 100 μm. For all in vitro studies, n $\geq$ 3. The data are represented as mean ± standard deviation (SD). Paired Student *t* test (*A, B, D*), 1-way analysis of variance (ANOVA) with Bonferroni test (*K, N, P*) or Tukey test (*F*), 2-way ANOVA with Bonferroni test (*M*), log-rank test (*H–I*), $^{*}P < .05$, $^{**}P < .01$, and $^{***}P < .001$.

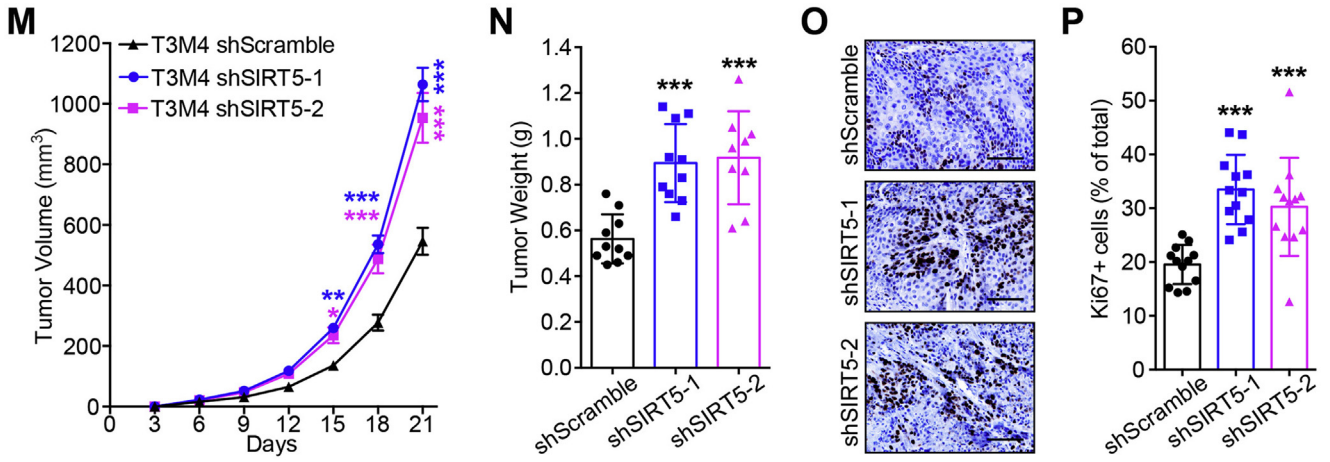

Figure 1. *Continued.*

Rockville, MD). The T3M4, S2-007, HPAF-II, Patu8902, Colo 357 (FG), and S2-013 cell lines were provided by Dr Michael A. Hollingsworth (Eppley Institute, University of Nebraska Medical Center [UNMC], Omaha, NE). The murine PDAC cell lines KPC1245 derived from $Kras^{G12D/+}$, $p53^{R172H/+}$, $Pdx1\text{-}Cre^{tg/+}$ (KPC) mice were provided by Dr David Tuveson (Cold Spring Harbor Laboratory; CSHL). Mouse PDAC cell lines KPC7460, KPC7472, and KPCS8508, KPCS8009 were derived from KPC and KPCS mice, respectively. Cells were cultured in Dulbecco's Modified Eagle Medium (DMEM) supplemented with 10% fetal bovine serum and 1% penicillin-streptomycin and incubated at 37°C in a 5% CO_2-humidified incubator. The cells were

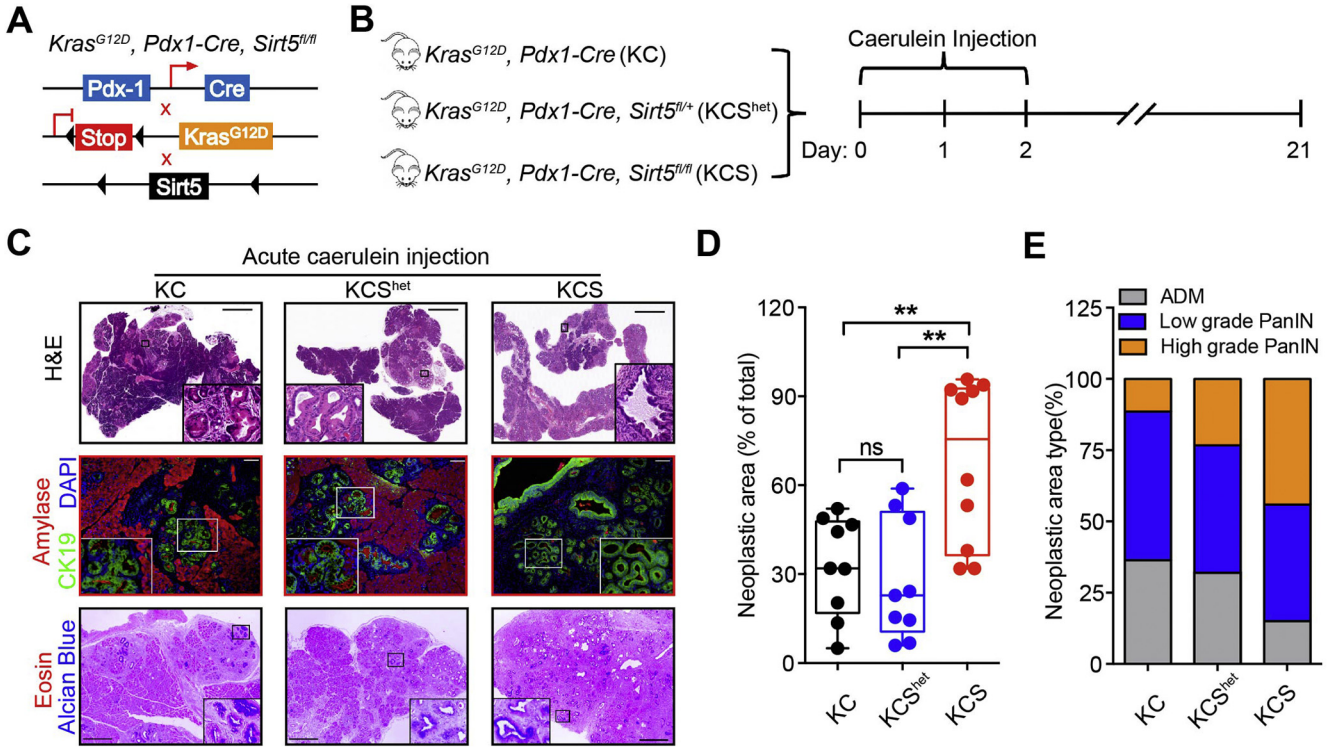

Figure 2. Sirt5 deficiency accelerates acinar-to-ductal metaplasia, PanIN formation, and pancreatic tumorigenesis. Cre: *Pdx1-Cre*; KC: $Kras^{G12D}$, *Pdx1-Cre*; KCS^{het}: $Kras^{G12D}$, *Pdx1-Cre*, $Sirt5^{fl/+}$; KCS: $Kras^{G12D}$, *Pdx1-Cre*, $Sirt5^{fl/fl}$. (*A*) Genetic strategy for investigating the function of Sirt5 in $Kras^{G12D}$-driven pancreatic tumorigenesis. (*B*) Intraperitoneally caerulein-injected KC (n = 9), KCS^{het} (n = 9), and KCS (n = 10) mice were euthanized at day 21. (*C*) H&E, CK19/Amylase, and Alcian blue/eosin staining of pancreatic tissue from caerulein-injected KC, KCS^{het}, and KCS mice. Scale bars 2000 μm (H&E), 100 μm (immunofluorescence), or 500 μm (Alcian blue/eosin staining). (*D*) The percentage of total PanIN area over the whole pancreatic tissue section from caerulein-treated mice. (*E*) Histopathologic analysis of pancreatic tissue sections from caerulein-treated mice. (*F* and *I*) H&E, CK19/Amylase, and Alcian blue/eosin staining of pancreatic tissue sections from 4-month-old (*F*) and 8-month-old (*I*) KC, KCS^{het}, and KCS mice. (*G*) Percentage of PanIN lesions over the whole pancreatic tissue section from 4-month-old KC (n = 5), KCS^{het} (n = 5), and KCS mice (n = 6). (*H* and *K*) Histopathologic analysis of 4-month-old (*H*) and 8-month-old (*K*) KC, KCS^{het}, and KCS mice tissue slides. (*J*) Percentage of PanIN lesion area over the whole pancreatic tissue section from 8-month-old KC (n = 6), KCS^{het} (n = 6), and KCS mice (n = 6). The data are represented as mean ± SD. One-way ANOVA with Tukey test was used for all panels, $^{*}P < .05$, $^{**}P < .01$, and $^{***}P < .001$.

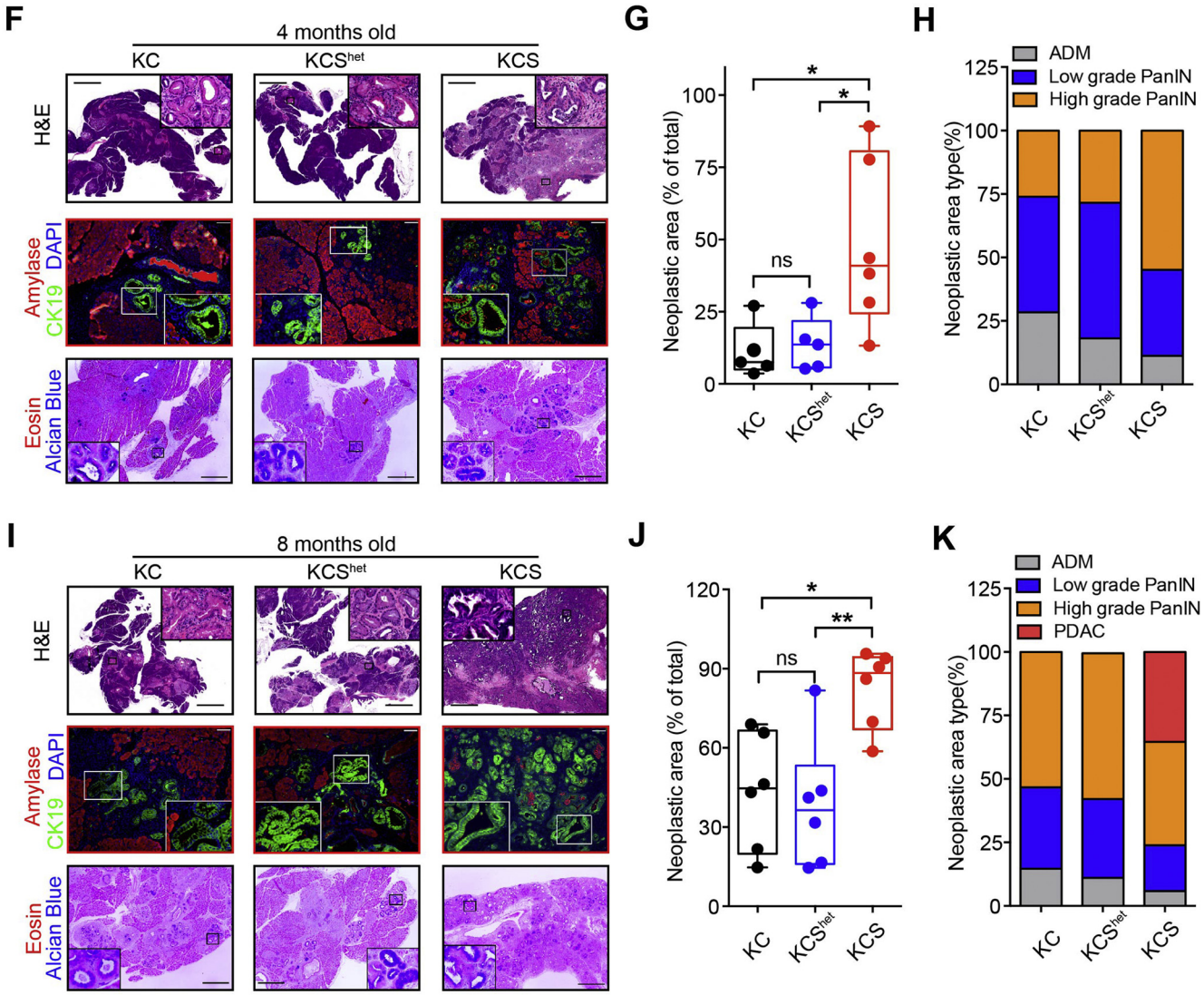

Figure 2. *Continued.*

authenticated using Short Tandem Repeat (STR) profiling and tested for mycoplasma contamination using a polymerase chain reaction (PCR)-based Mycoplasma Detection Kit.

Human Studies

The UNMC Tissue Bank provided the pancreatic cancer tissues used for PanIN and tumor progression studies, and PDX models. The UNMC Institutional Review Board Committee approved the studies related to the use of human samples for IHC in pancreatic intraepithelial neoplasia (PanIN) lesions. The UNMC Institutional Review Board Committee also approved the informed consent waiver. The pancreatic cancer tissue microarray used for survival analysis was obtained from Shanghai Outdo Biotech (Shanghai, China).

Mouse Strain Generation

The conditional *LSL-Kras*^{G12D}, *Pdx1-Cre*,[20] and *LSL-Tp53*^{R172H} [21] stains were purchased from the National Cancer Institute. Floxed *Sirt5* (*Sirt5*$^{fl/fl}$) mice were provided by Dr Johan Auwerx.[22] These mice strains were interbred to produce the following experimental cohorts: *Pdx1-Cre, Sirt5*$^{fl/fl}$ (CS); *Pdx1-Cre, LSL-Kras*^{G12D} (KC); *Pdx1-Cre, LSL-Kras*^{G12D}, *Sirt5*$^{fl/fl}$ (KCS); *Pdx1-Cre, LSL-Kras*^{G12D}, *LSL-Tp53*^{R172H} (KPC); and *Pdx1-Cre, LSL-Kras*^{G12D}, *LSL-Tp53*^{R172H}, *Sirt5*$^{fl/fl}$ (KPCS). For *Sirt5* loss-of-function studies, wild-type, *Sirt5*$^{fl/fl}$, or Pdx1-Cre littermates were used as controls. These experiment cohort strains were genotyped using PCR amplification methods. PCR primers used in genotyping are listed in Supplementary Table 4. For caerulein-induced pancreatitis, 7-week-old mice of indicated genotypes were intraperitoneally injected with caerulein (50 μg/kg) for 2 consecutive days every hour for 6 hours each day.

Additional methods are provided in the Supplementary Material.

Results

SIRT5 Down-Regulation Correlates With Disease Progression, Adverse Patient Outcomes, and Increased Tumor Cell Growth

The sirtuin family of proteins represents an important node in the regulation of cellular transcriptional response when presented with systemic metabolic cues or metabolic/

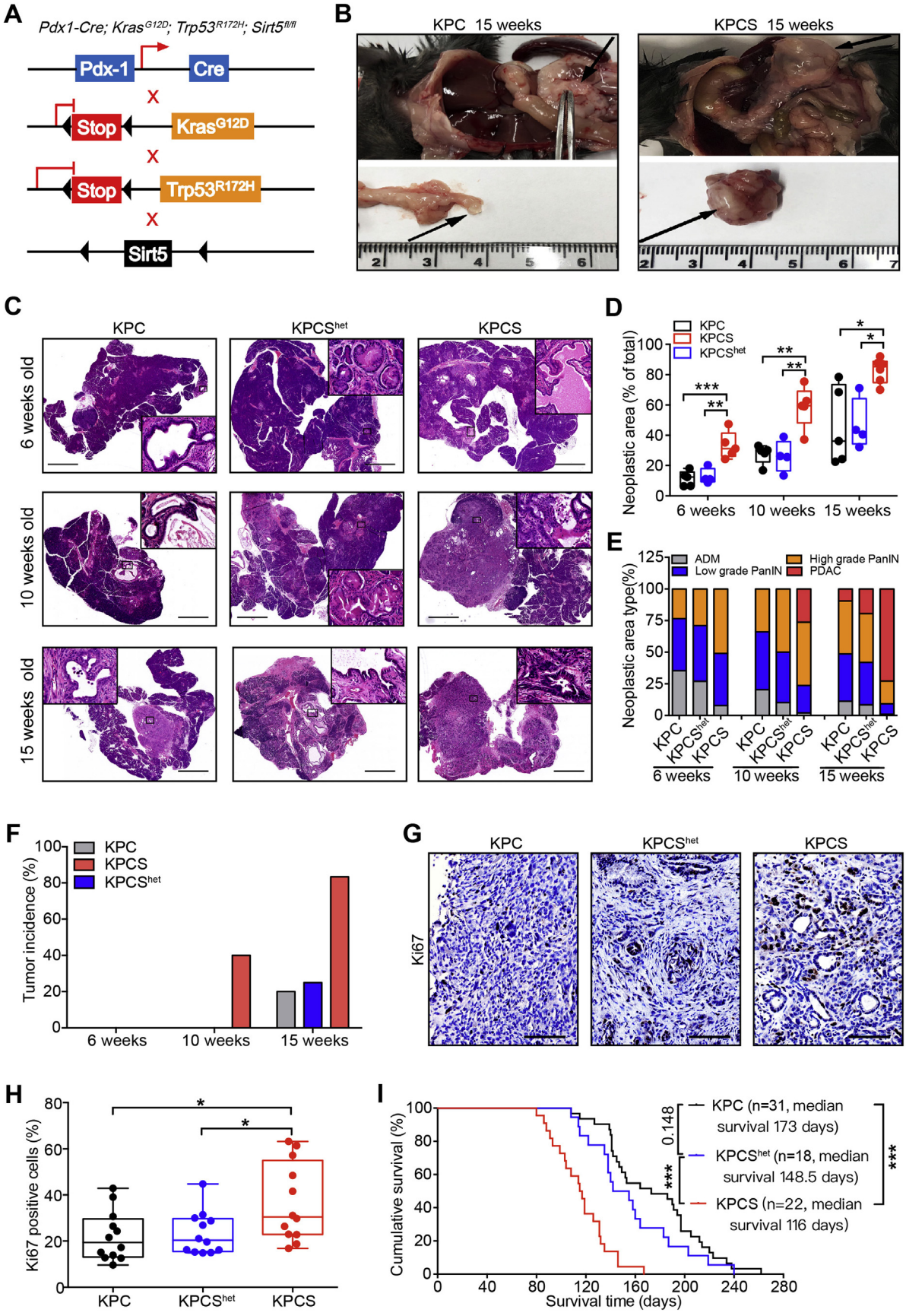
A
Pdx1-Cre; KrasG12D; Trp53R172H; Sirt5fl/fl
Pdx-1
Cre
Stop
KrasG12D
Stop
Trp53R172H
Sirt5
B
KPC 15 weeks
KPCS 15 weeks
C
KPC
KPCShet
KPCS
6 weeks old
10 weeks old
15 weeks old
D
KPC
KPCS
KPCShet
Neoplastic area (% of total)
6 weeks
10 weeks
15 weeks
E
ADM
Low grade PanIN
High grade PanIN
PDAC
Neoplastic area type(%)
KPC
KPCShet
KPCS
6 weeks
10 weeks
15 weeks
F
KPC
KPCS
KPCShet
Tumor incidence (%)
6 weeks
10 weeks
15 weeks
G
KPC
KPCShet
KPCS
Ki67
H
Ki67 positive cells (%)
KPC
KPCShet
KPCS
I
Cumulative survival (%)
KPC (n=31, median survival 173 days)
KPCShet (n=18, median survival 148.5 days)
KPCS (n=22, median survival 116 days)
0.148
***
***
Survival time (days)

nutritional changes.[23] To investigate whether sirtuins are dysregulated in PDAC, the present study evaluated the messenger RNA (mRNA) expression of all the 7 sirtuins in matched human normal and PDAC tissues from the GEO database (GDS4103). Results showed that expression levels of *SIRT3*, *SIRT5*, and *SIRT6* were significantly decreased in PDAC tissues, whereas expression levels of *SIRT1* and *SIRT7* were remarkably increased in PDAC (Figure 1*A*, Supplementary Figure 1*A–F*). Among the dysregulated sirtuins, *SIRT5* remains the only sirtuin that has not been investigated for its role in PDAC. To corroborate the expression data from GEO, the public database Oncomine was queried and that further showed SIRT5 expression to be downregulated in PDAC tissues (Supplementary Figure 1*G–H*).

To establish whether SIRT5 plays a causative role in the pathogenesis of PDAC, we used the autochthonous *LSL-Kras^{G12D}*; *LSL-Trp53^{R172H}*; *Pdx1-Cre* (KPC) mouse model and observed that *Sirt5* mRNA and protein levels were significantly decreased in KPC pancreatic cancer tissues compared with the age-matched normal pancreas tissues (Figure 1*B–D*). A decrease in SIRT5 expression was noted during the progression from adjacent normal tissues to PanIN and PDAC in KPC mouse models (Supplementary Figure 1*I–J*) and human samples (Figure 1*E–F*). Furthermore, low-SIRT5 expression correlated with tumor recurrence in human patients (Supplementary Table 1). Low expression of SIRT5 was associated with decreased survival of patients with PDAC (Figure 1*G–I*). Moreover, low-SIRT5 expression independently correlated with high mortality risk in patients with PDAC (Supplementary Figure 1*E* and Supplementary Tables 1–3).

To examine the effect of SIRT5 on PDAC aggressiveness, SIRT5 expression was evaluated in 13 PDAC cell lines (Supplementary Figure 1*L*). Cells with relatively high expression of SIRT5 (ie, T3M4, Capan2, PANC1, and S2-007) were used to generate stable *SIRT5* knockdowns, whereas those with low SIRT5 (ie, S2-013 and Capan1) were chosen to generate *SIRT5*-overexpressing cell lines. The efficiency of *SIRT5* knockdown and overexpression was verified using quantitative PCR and immunoblotting (Supplementary Figure 1*M–Q*). *SIRT5* knockdown enhanced PDAC cell proliferation, colony formation, and sphere formation (Supplementary Figure 2*A–L*). Conversely, *SIRT5* overexpression inhibited PDAC cell growth, whereas the catalytically inactive mutant SIRT5-H158Y[11] did not exhibit significant inhibitory effects on PDAC cell growth (Supplementary Figure 2*M–P*). The expression levels of SIRT5 were also investigated in a panel of 6 human PDAC tumor-derived organoid lines, and *SIRT5* expression was knocked down in the PA901 and PA717 organoids with high endogenous SIRT5 levels (Supplementary Figure 1*R–S*). Knockdown of *SIRT5* also increased human PDAC organoid growth (Figure 1*J–K*). Moreover, *SIRT5* knockdown accelerated T3M4 tumor growth upon orthotopic implantation (Figure 1*L–P*).

Genetic Ablation of Sirt5 *Promotes Pancreatic Tumorigenesis in Cooperation With Oncogenic Mutations*

To determine the role of SIRT5 in PDAC pathogenesis, genetically engineered mice were generated that carried pancreas-specific ablation of *Sirt5,* along with oncogenic mutations in *Kras* alone or *Kras* and *Trp53*. *Pdx1-Cre*; *Sirt5$^{fl/fl}$* (CS) were generated by crossing *Pdx1-Cre* mice with *Sirt5$^{fl/fl}$* mice (Supplementary Figure 3*A–B*). As controls, histologic analysis of pancreata isolated from CS and *Pdx1-Cre* mice did not show any apparent abnormalities (Supplementary Figure 3*C–D*). Furthermore, there was no significant difference in the body weight changes between these 2 groups (Supplementary Figure 3*E*). *Kras^{G12D}*; *Sirt5$^{fl/fl}$* mice were crossed with *Pdx1-Cre*; *Sirt5$^{fl/+}$* mice to generate mice with mutant *Kras* and heterozygous/homozygous *Sirt5* loss, ie, *Pdx1-Cre*; *Kras^{G12D}*; *Sirt5$^{fl/+}$*; (KCS^{het}) and *Pdx1-Cre*; *Kras^{G12D}*; *Sirt5$^{fl/fl}$* (KCS), respectively (Supplementary Figure 3*A–B* and Figure 2*A*). The cholecystokinin analog caerulein is a widely used drug to induce pancreatitis.[24] Wild type, Pdx1-Cre, and CS mice exhibited expected overall nontransformed pancreatic histology 21 days post–caerulein injection (Supplementary Figure 4*A–B*). Conversely, KCS mice had a larger neoplastic area, increased acinar cell loss (decreased amylase positivity and increased CK19 positivity), and more high-grade PanIN lesions than the *Pdx1-Cre*; *Kras^{G12D}* (KC) and KCS^{het} mice (Figure 2*B–E*). SIRT5 IHC staining of pancreatic tissue from KCS mice confirmed the efficient deletion of *Sirt5* (Supplementary Figure 4*C*). Lesions from the KCS mice displayed a significantly enhanced cell proliferation index, as indicated by increased Ki67-staining (Supplementary Figure 4*C–D*). Thus, *Sirt5* deletion accelerates *Kras^{G12D}*-triggered pancreatic tumorigenesis in the context of a caerulein-induced pancreatitis model.

Next, the role of Sirt5 in *Kras^{G12D}*-triggered pancreatic tumorigenesis was examined in the absence of caerulein. The pancreata from 4-month-old KCS mice exhibited significantly larger neoplastic areas as well as higher-grade PanIN lesions compared with age-matched KC and KCS^{het} mice (Figure 2*F–H*). Ki67 staining results showed that the PanIN ductal cells from KCS mice exhibited an enhanced proliferative index (Supplementary Figure 4*E–F*). To

Figure 3. Genomic ablation of *Sirt5* promotes PDAC progression. (*A*) Genetic strategy for investigating the function of the *Sirt5* in *Kras^{G12D}* and *Trp53^{R172H}*-driven pancreatic tumorigenesis. (*B*) Representative images of pancreatic tumors in 15-week-old KPC and KPCS mice. (*C*) Representative H&E-stained images of the pancreatic tissue from age-matched KPC (n = 5), KPCS^{het} (n = 4), and KPCS (n = 5) mice at 6, 10, and 15 weeks. Scale bars 2000 μm. (*D*) Percentage of PanIN and PDAC lesion area over the whole pancreatic tissue sections from KPC, KPCS^{het}, and KPCS mice at the indicated age. (*E*) Histopathologic analysis of pancreatic tissues from KPC, KPCS^{het}, and KPCS mice at indicated age. (*F*) Tumor incidence in KPC, KPCS^{het}, and KPCS cohorts at the indicated age. (*G–H*) Ki67 staining and quantification in pancreatic tumor tissues from KPC, KPCS^{het}, and KPCS mice. Scale bars 100 μm. (*I*) Kaplan-Meier survival analysis of the KPC, KPCS^{het}, and KPCS mice (log-rank test). The data are represented as mean ± SD. One-way ANOVA with Tukey test for panels *D* and *H*, $^{*}P < .05$, $^{**}P < .01$, and $^{***}P < .001$.

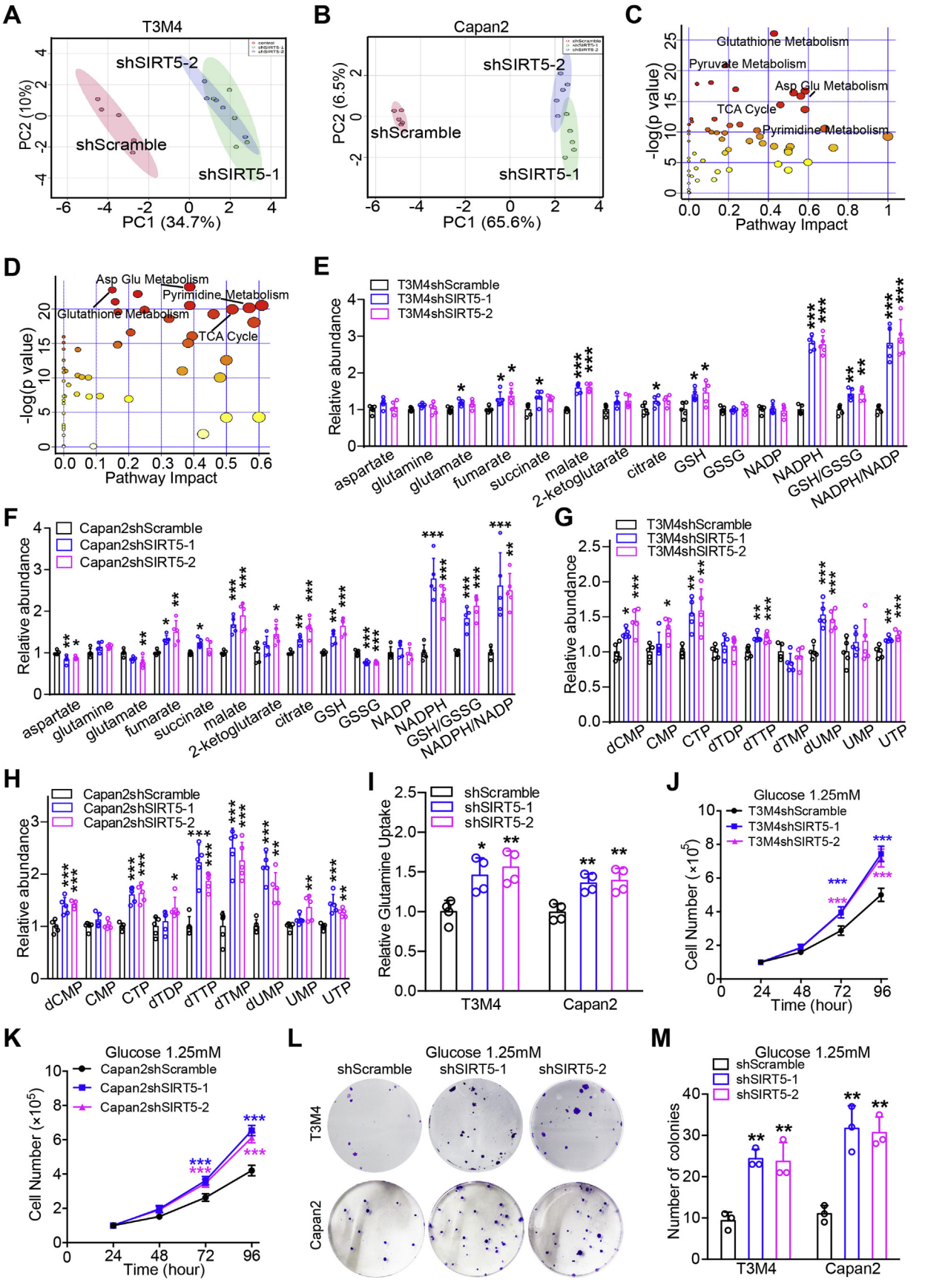
A
T3M4
shSIRT5-2
shScramble
shSIRT5-1
PC2 (10%)
PC1 (34.7%)
B
Capan2
shSIRT5-2
shScramble
shSIRT5-1
PC2 (6.5%)
PC1 (65.6%)
C
Glutathione Metabolism
Pyruvate Metabolism
Asp Glu Metabolism
TCA Cycle
Pyrimidine Metabolism
-log(p value)
Pathway Impact
D
Asp Glu Metabolism
Pyrimidine Metabolism
Glutathione Metabolism
TCA Cycle
-log(p value)
Pathway Impact
E
T3M4shScramble
T3M4shSIRT5-1
T3M4shSIRT5-2
Relative abundance
aspartate
glutamine
glutamate
fumarate
succinate
malate
2-ketoglutarate
citrate
GSH
GSSG
NADP
NADPH
GSH/GSSG
NADPH/NADP
F
Capan2shScramble
Capan2shSIRT5-1
Capan2shSIRT5-2
Relative abundance
aspartate
glutamine
glutamate
fumarate
succinate
malate
2-ketoglutarate
citrate
GSH
GSSG
NADP
NADPH
GSH/GSSG
NADPH/NADP
G
T3M4shScramble
T3M4shSIRT5-1
T3M4shSIRT5-2
Relative abundance
dCMP
CMP
CTP
dTDP
dTTP
dTMP
dUMP
UMP
UTP
H
Capan2shScramble
Capan2shSIRT5-1
Capan2shSIRT5-2
Relative abundance
dCMP
CMP
CTP
dTDP
dTTP
dTMP
dUMP
UMP
UTP
I
shScramble
shSIRT5-1
shSIRT5-2
Relative Glutamine Uptake
T3M4
Capan2
J
Glucose 1.25mM
T3M4shScramble
T3M4shSIRT5-1
T3M4shSIRT5-2
Cell Number (×10^5)
Time (hour)
K
Glucose 1.25mM
Capan2shScramble
Capan2shSIRT5-1
Capan2shSIRT5-2
Cell Number (×10^5)
Time (hour)
L
Glucose 1.25mM
shScramble
shSIRT5-1
shSIRT5-2
T3M4
Capan2
M
Glucose 1.25mM
shScramble
shSIRT5-1
shSIRT5-2
Number of colonies
T3M4
Capan2

identify the role of Sirt5 at a later stage of $Kras^{G12D}$-triggered pancreatic tumorigenesis, pancreatic tissues were collected from 8-month-old KC, KCS^{het}, and KCS mice. All KCS mice obtained numerous PanIN lesions at the age of 8 months, and 2 of 6 KCS mice developed PDAC (Figure 2*I–K*). The area, grade, and proliferative potential of PanIN lesions in KC as well as KCS^{het} mice were significantly lower than the age-matched KCS mice (Figure 2*I–K*, Supplementary Figure 4*G–H*). These data indicate *Sirt5* loss facilitates the oncogenic $Kras^{G12D}$-driven initiation of pancreatic tumorigenesis in the absence of caerulein.

To further examine the effect of Sirt5 deficiency on pancreatic cancer progression and survival, KPC (*Pdx1-Cre*; $Kras^{G12D}$; $Trp53^{R172H}$) mice with heterozygous/homozygous *Sirt5* loss (*Pdx1-Cre*; $Kras^{G12D}$; $Trp53^{R172H}$; $Sirt5^{fl/+}$, $KPCS^{het}$ and *Pdx1-Cre*; $Kras^{G12D}$; $Trp53^{R172H}$; $Sirt5^{fl/fl}$, *KPCS*) were generated (Supplementary Figure 3*A–B* and Figure 3*A*). KPCS mice at 15 weeks of age developed large intraperitoneal pancreatic tumor masses, whereas the corresponding age-matched KPC mice had only small pancreatic tumor nodules (Figure 3*B*). Age-matched KPC and KPCS mice were assessed at different time points to monitor the pancreatic tumorigenesis (Figure 3*C*). At 6 weeks, KPCS mice had a significantly increased percentage of neoplastic area, and more than half of the KPCS mice exhibited high-grade PanIN, which was significantly faster than the age-matched KPC and $KPCS^{het}$ mice (Figure 3*C–E*). Complete scans of pancreatic tissue sections indicated that pancreatic tumors developed in KPCS mice as early as 10 weeks (40%). Moreover, 5 of 6 15-week-old KPCS mice developed pancreatic cancer (Figure 3*F*). Furthermore, Ki67 staining results demonstrated *Sirt5* deletion significantly promoted pancreatic cancer cell proliferation (Figure 3*G–H*). Because *Sirt5* deletion in mice with the KPC background accelerated pancreatic cancer progression, KPC, $KPCS^{het}$, and KPCS mice were then used to investigate the impact of *Sirt5* loss on survival. The KPCS mice had a dramatically shortened median survival time at 116 days, whereas the median survival times of KPC and $KPCS^{het}$ mice were 173 days and 148.5 days, respectively (Figure 3*I*). Therefore, *Sirt5* deletion, in cooperation with *Kras* and *Tp53* mutations, accelerates pancreatic cancer progression and shortens the survival time of the spontaneous PDAC progression mouse model.

SIRT5 Modulates Pancreatic Cancer Cell Growth by Suppressing Glutamine and Glutathione Metabolism

Previous studies have demonstrated that SIRT5 regulated tumorigenesis of multiple cancer types by mediating their metabolic reprogramming.[12–16] As such, the present study next investigated whether SIRT5 could regulate PDAC metabolism. liquid chromatography-coupled tandem-mass spectrometry (LC-MS/MS)-based metabolite profiles revealed distinct metabolic alterations between control and *SIRT5*-knockdown PDAC cells (Figure 4*A–B*, Supplementary Figure 5). Moreover, metabolite set enrichment analysis indicated that *SIRT5* knockdown led to significant changes in metabolites involved in glutathione metabolism, glutamine metabolism, pyrimidine metabolism, and the tricarboxylic acid cycle (Figure 4*C–D*). *SIRT5*-knockdown significantly increased the relative abundance of glutamine metabolism intermediates (ie, malate, fumarate, and citrate), glutathione metabolism pathway metabolites (ie, reduced glutathione (GSH) and NADPH), and the pyrimidine metabolism intermediates (ie, deoxycytidine monophosphate [dCMP], cytidine triphosphate [CTP], deoxythymidine triphosphate [dTTP], deoxyuridine monophosphate [dUMP], uridine triphosphate [UTP]) (Figure 4*E–H*, Supplementary Figure 5*A–B*). *SIRT5*-knockdown also led to increased reduction potential as noted by increased reduced glutathione/oxidized glutathione ratio (GSH/GSSG) and NADPH/nicotinamide adenine dinucleotide phosphate (NADP) ratios (Figure 4*E–F*). Furthermore, the glutamine uptake was measured in control and *SIRT5*-knockdown PDAC cells. These assays revealed the uptake of glutamine remarkably increased in *SIRT5*-knockdown cells (Figure 4*I*). Interestingly, the differences in cell growth rates between the control and *SIRT5*-knockdown PDAC cells were much greater under the low-glucose (1.25 mmol/L; 5%) conditions than those in normal culture conditions (Figure 4*J–M*). These data suggest *SIRT5* loss increases glutamine use to maintain redox balance and support PDAC cell growth even under glucose-limited conditions.

SIRT5 Induces Dysregulated Glutamine and Glutathione Metabolism via GOT1

Next, we investigated the mechanistic basis of SIRT5-mediated dysregulation of glutamine and glutathione metabolism in PDAC. *KRAS*-mutated PDAC cells rely on noncanonic glutamine metabolism (Figure 5*A*).[5] There were no significant differences in mRNA or protein levels of noncanonic glutamine metabolic pathway enzymes upon *SIRT5* knockdown (Supplementary Figure 6*A–C*). As such, the present study measured the enzymatic activities of enzymes including glutaminase (GLS), GLUD1, and GOT from control and *SIRT5*-knockdown PDAC cell extracts. Interestingly, suppression of SIRT5 in PDAC cells significantly promoted the enzyme activity of GOT, but not GLS or GLUD1

Figure 4. SIRT5 suppresses glutamine and glutathione metabolism, and regulates cellular redox homeostasis. (*A–B*). Principal component analysis of metabolic profiles from control and *SIRT5*-knockdown cells (N = 5). (*C–D*) Metabolic pathway analysis of significantly dysregulated metabolites in control and *SIRT5*-knockdown cells. (*E–F*) Significantly different metabolites in glutamine and glutathione metabolism from control and *SIRT5*-knockdown cells. (*G–H*) Significantly different metabolites in pyrimidine metabolism from control and *SIRT5*-knockdown cells. (*I*) Relative glutamine uptake in control and *SIRT5*-knockdown cells. (*J–K*) Growth curves of control and *SIRT5*-knockdown cells cultured under low-glucose conditions (1.25 mmol/L). (*L–M*) Colony formation assays for control and *SIRT5*-knockdown cells under low-glucose conditions (1.25 mmol/L). For all in vitro studies, N $\geq$ 3. The data are represented as mean ± SD. One-way ANOVA with Bonferroni test (*E–I*, *M*), 2-way ANOVA with Bonferroni test (*J–K*), **P* < .05, ***P* < .01, and ****P* < .001.

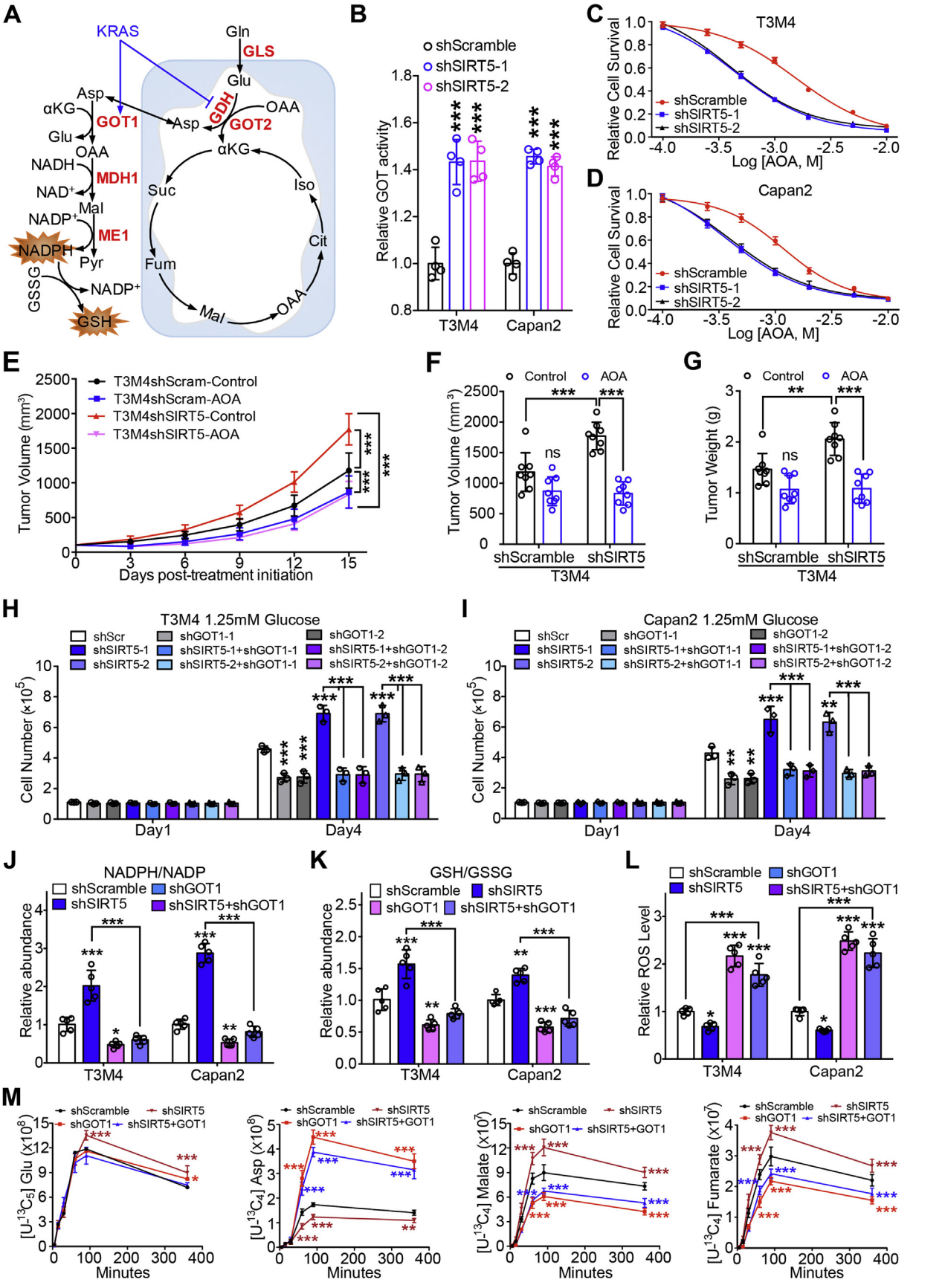
A
KRAS
Gln
GLS
Glu
Asp
αKG
GOT1
GDH
OAA
GOT2
Glu
OAA
NADH
MDH1
NAD+
Mal
NADP+
ME1
NADPH
Pyr
GSSG
NADP+
GSH
Suc
Iso
Cit
Fum
Mal
OAA
B
shScramble
shSIRT5-1
shSIRT5-2
Relative GOT activity
T3M4
Capan2
C
T3M4
Relative Cell Survival
shScramble
shSIRT5-1
shSIRT5-2
Log [AOA, M]
D
Capan2
Relative Cell Survival
shScramble
shSIRT5-1
shSIRT5-2
Log [AOA, M]
E
T3M4shScram-Control
T3M4shScram-AOA
T3M4shSIRT5-Control
T3M4shSIRT5-AOA
Tumor Volume (mm3)
Days post-treatment initiation
F
Control
AOA
Tumor Volume (mm3)
ns
shScramble
shSIRT5
T3M4
G
Control
AOA
Tumor Weight (g)
ns
shScramble
shSIRT5
T3M4
H
T3M4 1.25mM Glucose
shScr
shSIRT5-1
shSIRT5-2
shGOT1-1
shSIRT5-1+shGOT1-1
shSIRT5-2+shGOT1-1
shGOT1-2
shSIRT5-1+shGOT1-2
shSIRT5-2+shGOT1-2
Cell Number (×10^5)
Day1
Day4
I
Capan2 1.25mM Glucose
shScr
shSIRT5-1
shSIRT5-2
shGOT1-1
shSIRT5-1+shGOT1-1
shSIRT5-2+shGOT1-1
shGOT1-2
shSIRT5-1+shGOT1-2
shSIRT5-2+shGOT1-2
Cell Number (×10^5)
Day1
Day4
J
NADPH/NADP
shScramble
shSIRT5
shGOT1
shSIRT5+shGOT1
Relative abundance
T3M4
Capan2
K
GSH/GSSG
shScramble
shSIRT5
shGOT1
shSIRT5+shGOT1
Relative abundance
T3M4
Capan2
L
shScramble
shSIRT5
shGOT1
shSIRT5+shGOT1
Relative ROS Level
T3M4
Capan2
M
shScramble
shSIRT5
shGOT1
shSIRT5+GOT1
[U-13C5] Glu (x10^8)
Minutes
shScramble
shSIRT5
shGOT1
shSIRT5+GOT1
[U-13C4] Asp (x10^8)
Minutes
shScramble
shSIRT5
shGOT1
shSIRT5+GOT1
[U-13C4] Malate (x10^7)
Minutes
shScramble
shSIRT5
shGOT1
shSIRT5+GOT1
[U-13C4] Fumarate (x10^7)
Minutes

(Figure 5*B* and Supplementary Figure 6*D–E*). Next, the control and *SIRT5*-knockdown PDAC cells were treated with inhibitors of glutamine pathway metabolic enzymes to examine their selective responsiveness to these inhibitors (Supplementary Figure 6*F*). Results showed *SIRT5*-knockdown PDAC cells were more sensitive to GOT-inhibitor aminooxyacetate (AOA) than control cells (Figure 5*C–D*), but there was no significant difference between control and *SIRT5*-knockdown cells when treated with GLS-inhibitor BPTES and GLUD1-inhibitor EGCG (Supplementary Figure 6*G–J*). Moreover, orthotopic implantation studies demonstrated *SIRT5*-knockdown T3M4 cells were more vulnerable to AOA treatment (Figure 5*E–G*, Supplementary Figure 6*K–L*). These data indicate SIRT5 inhibits glutamine/glutathione metabolism primarily by suppressing the enzyme activity of GOT.

To further identify which GOT isoform (GOT1 or GOT2) is the primary target of SIRT5, *GOT1* and *GOT2* were knocked down in both control and *SIRT5*-knockdown PDAC cells (Supplementary Figure 6*M–P*). *GOT1* silencing abolished *SIRT5*-knockdown-induced PDAC cell growth (Figure 5*H–I*), whereas knockdown of *GOT2* did not significantly affect cell growth in all of the *SIRT5*-knockdown cells under low-glucose (1.25 mmol/L) conditions (Supplementary Figure 6*Q–R*). These data preliminarily indicate that GOT1 plays a major role in *SIRT5*-loss–mediated cell growth. To confirm the regulation of GOT1 by SIRT5, metabolites from control, *GOT1*-knockdown, *SIRT5*-knockdown, and *SIRT5/GOT1*-double-knockdown cells were subjected to LC-MS/MS-based metabolomic analysis. *SIRT5*-knockdown cells demonstrated significantly increased ratios of reduced-glutathione to oxidized-glutathione (GSH/GSSG) and cellular reduced nicotinamide adenine dinucleotide phosphate/oxidized nicotinamide adenine dinucleotide phosphate (NADPH/NADP), which was abolished by *GOT1* knockdown (Figure 5*J–K*). GOT1 catalyzes the conversion reactions of 2-ketoglutarate and aspartate into glutamate and oxaloacetate. The metabolomics data indicated *SIRT5* knockdown increased the abundance of the GOT1 downstream intermediates (ie, malate, fumarate). Contrastingly, *SIRT5*-loss–induced increase in malate and fumarate levels was abolished by the *GOT1* knockdown, with a concomitant increase in the levels of the precursor metabolite 2-ketoglutarate (Supplementary Figure 6*S-T*). As the reducing equivalent NADPH and GSH are important for cellular redox homeostasis, *SIRT5* knockdown was posited to increase the generation of NADPH and GSH to maintain redox balance and promote cell proliferation in PDAC cells. As expected, *GOT1* silencing abrogated a *SIRT5*-knockdown–mediated decrease of the intracellular reactive oxygen species (ROS) levels (Figure 5*L*). Furthermore, [U-$^{13}C_5$] glutamine-based kinetic flux analysis demonstrated *SIRT5* knockdown significantly increased levels of ^{13}C-labeled malate and fumarate; these increased levels were abolished by *GOT1* knockdown (Figure 5*M*). Taken together, these findings indicate that SIRT5 inhibits glutamine/glutathione metabolism and regulates cellular redox homeostasis by attenuating the enzymatic activity of GOT1.

SIRT5 Inhibits GOT1 Enzymatic Activity by Catalyzing its Lysine Deacetylation

We then investigated the mechanistic basis of SIRT5-mediated modulation of GOT1 activity. Considering SIRT5 has been found to regulate metabolic enzymatic activity by altering the post-translational modifications in enzymes,[11,25–28] the present study examined whether SIRT5 potentially catalyzes lysine post-translational modifications in GOT1. Interestingly, the lysine acetylation level of GOT1 decreased upon SIRT5 overexpression in PDAC cells, whereas the lysine glutarylation, succinylation, or malonylation levels of GOT1 remained unaltered or undetectable (Figure 6*A*). In contrast, *SIRT5*-knockdown significantly increased the acetylation level of both exogenous GOT1 (Figure 6*B*) and endogenous GOT1 (Supplementary Figure 7*A*). Moreover, the catalytically inactive mutant SIRT5-H158Y[11] failed to induce the deacetylation of GOT1 protein compared with the wild-type SIRT5 (Figure 6*C*). To further identify the SIRT5-dependent deacetylation sites on GOT1, GOT1 protein was purified from the control and *SIRT5*-knockdown T3M4 cells, and post-translational modifications were assessed using mass spectrometry. As shown in Figure 6*D* and Supplementary Figure 7*B–G*, 3 acetylation sites (lysine 276, lysine 290, and lysine 369) were found in both control and *SIRT5*-knockdown cells. In addition, a

Figure 5. SIRT5 inhibits glutamine and glutathione metabolism by decreasing GOT1 enzyme activity. (*A*) The schematic illustration of the Kras-regulated glutamine and glutathione metabolism in mutant Kras-driven PDAC. (*B*) Relative GOT enzyme activity in control and *SIRT5*-knockdown cells. (*C–D*) Relative survival of control and *SIRT5*-knockdown cells treated with GOT inhibitor AOA. Data are normalized to the respective untreated group. (*E–G*) Effect of AOA treatment on T3M4 shScramble and *shSIRT5* cells in vivo. Tumor growth rates at indicated time points (*E*). Tumor volume (*F*) and tumor weight in each group upon necropsy (*G*). (*H–I*) Cell growth of control and *SIRT5*-knockdown cells transfected with control or *GOT1* short hairpin RNA (shRNA) under low-glucose conditions (1.25 mmol/L). Experiments for scrambled control and *SIRT5*-knockdown cells transfected with *GOT1* or *GOT2* shRNA were set up together with common controls. (*J–K*) Relative reduced nicotinamide adenine dinucleotide phosphate/oxidized nicotinamide adenine dinucleotide phosphate (NADPH/NADP) ratio (*J*) or GSH/GSSG ratio (*K*) in control, *GOT1*-knockdown, *SIRT5*-knockdown, and *SIRT5/GOT1*-double-knockdown cells. GSH, reduced glutathione; GSSH, oxidized glutathione. (*L*) Relative intracellular reactive oxygen species (ROS) levels in the indicated cells. ROS-insensitive carboxy-DCFDA (CDCFDA) dye was used as a negative control. (*M*) Kinetic flux analysis of ^{13}C-labeled glutamine carbon incorporation into downstream metabolites in control, *GOT1*-knockdown, *SIRT5*-knockdown, and *SIRT5/GOT1*-double-knockdown T3M4 cells. Asp, aspartate; Glu, glutamate. For all in vitro studies, N $\geq$ 3. The data are represented as mean $\pm$ SD. One-way ANOVA with Bonferroni test (*B*) or Tukey test (*F–L*), 2-way ANOVA with Tukey test (*E*) or Bonferroni test (*M*), $^{*}P < .05$, $^{**}P < .01$, and $^{***}P < .001$.

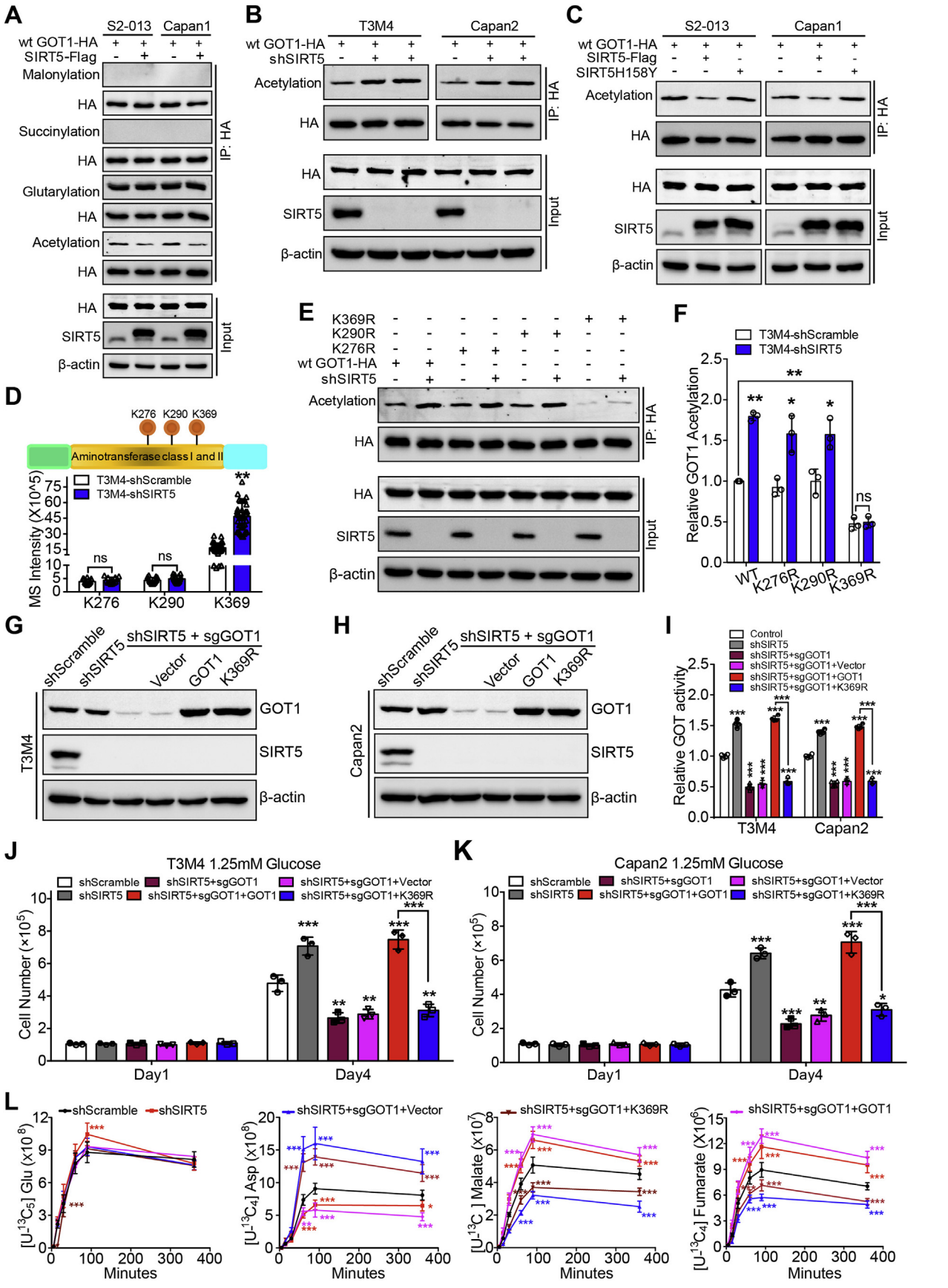
A
S2-013
Capan1
wt GOT1-HA
SIRT5-Flag
Malonylation
Succinylation
Glutarylation
Acetylation
HA
IP: HA
SIRT5
β-actin
Input
B
T3M4
Capan2
shSIRT5
C
SIRT5H158Y
D
K276 K290 K369
Aminotransferase class I and II
T3M4-shScramble
T3M4-shSIRT5
MS Intensity (X10^5)
ns
E
K369R
K290R
K276R
F
Relative GOT1 Acetylation
WT
G
shScramble
shSIRT5
shSIRT5 + sgGOT1
Vector
GOT1
K369R
T3M4
H
Capan2
I
Control
shSIRT5
shSIRT5+sgGOT1
shSIRT5+sgGOT1+Vector
shSIRT5+sgGOT1+GOT1
shSIRT5+sgGOT1+K369R
Relative GOT activity
J
T3M4 1.25mM Glucose
Cell Number (×10^5)
Day1
Day4
K
Capan2 1.25mM Glucose
L
[U-13C5] Glu (x10^8)
[U-13C4] Asp (x10^8)
[U-13C] Malate (x10^7)
[U-13C4] Fumarate (X10^6)
Minutes

comparison of the lysine acetylation intensities of GOT1 between control and *SIRT5*-knockdown cells indicated lysine 369 as the major lysine target residue that SIRT5 deacetylates (Figure 6*D*).

To identify if SIRT5-catalyzed post-translational modifications of GOT1 regulated GOT1 activity, we performed site-directed mutagenesis. The lysine to arginine (ie, K-to-R) mutation preserves the positive charge but cannot be acetylated, and is frequently used as a deacylated lysine mimetic.[29] Hence, 3 mutant HA-tagged *GOT1* plasmids were generated, in which the lysine 276, lysine 290, or lysine 369 residues were substituted with arginine (R). The wild-type *GOT1* plasmid, *GOT1-K276R*, *GOT1-K290R*, and *GOT1-K369R* mutant plasmids were transfected into control and *SIRT5*-knockdown T3M4 cells. Immunoblots of the purified GOT1 protein from cells expressing wild-type GOT1, GOT1-K276R, GOT1-K290R, and GOT1-K369R mutants were used to detect the acetylation levels of GOT1. The K369R mutation resulted in a significant decrease in the acetylation level of GOT1 (Figure 6*E–F*). Furthermore, *SIRT5*-knockdown significantly increased the lysine acetylation levels of wild-type GOT1, GOT1-K276R, and GOT1-K290R mutants, but not the GOT1-K369R mutant (Figure 6*E–F*). These data indicate lysine 369 in GOT1 protein is the primary deacetylation target of SIRT5. To further evaluate the function of GOT1-K369 acetylation under *SIRT5*-knockdown conditions, first the CRISPR/Cas9 technique was used to generate *GOT1*-knockout/*SIRT5*-knockdown cells. The above *GOT1*-knockout/*SIRT5*-knockdown cells were then engineered to re-express vector, wild-type *GOT1*, or *GOT1-K369R* mutant plasmids (Figure 6*G–H*). *GOT1* knockout abolished *SIRT5*-knockdown–mediated increase of GOT enzymatic activity, while re-expressing wild-type GOT1, but not GOT1-K369R, restored this activity (Figure 6*I*). Thus, K369 deacetylation by SIRT5 is primarily responsible for SIRT5-mediated abrogation of GOT activity in PDAC cells.

GOT1 knockout inhibited the effects of *SIRT5*-knockdown on cell growth, whereas re-expression of wild-type GOT1 rescuedcell growth. However, re-expression of GOT1-K369R failed to restore cell growth in *GOT1*-knockout/*SIRT5*-knockdown PDAC cells under low-glucose (1.25 mmol/L) conditions (Figure 6*J–K*). Consistently, the [U-$^{13}C_5$] glutamine-based kinetic flux analysis indicated *GOT1* knockout abolished the increased ^{13}C-labeled malate and fumarate levels in *SIRT5*-knockdown cells. Moreover, re-expressing wild-type GOT1 could restore the ^{13}C-labeled malate and fumarate levels in *GOT1*-knockout/*SIRT5*-knockdown cells, whereas expressing GOT1-K369R was unable to rescue this phenomenon (Figure 6*L*). Taken together, these results strongly indicate that SIRT5 suppresses GOT1 enzymatic activity by deacetylating GOT1 at lysine 369, which leads to the inhibition of tumor cell growth.

Targeting PDAC With Small-Molecule SIRT5-Activator MC3138 Improves Therapeutic Efficiency

Given the important role of SIRT5 in the development of PDAC, it has the potential to serve as a promising drug target. A small-molecule SIRT5 activator, a 1,4-dihydropyridine, termed MC3138, was developed (Figure 7*A*) and tested for potential effects on human PDAC cell lines, organoids, and PDX tumors. The biochemical enzymatic assay results indicated that MC3138 exhibited a selective activation of SIRT5 compared with the selective SIRT1 activator SRT2104 and SIRT3 activator Honokiol (Supplementary Figure 8*A–C*). Moreover, treatment with MC3138 mimicked the deacetylation effect mediated by SIRT5 overexpression (Supplementary Figure 8*D*). MC3138 treatment decreased lysine acetylation of the GOT1 protein and inhibited its enzymatic activity (Figure 7*B–C*). The cell viability assay showed MC3138 reduced PDAC cell viability, with half maximal inhibitory concentration (IC50) values ranging from 25.4 μmol/L–236.9 μmol/L (Figure 7*D* and Supplementary Figure 8*E–F*). To validate whether the inhibitory effect of MC3138 was associated with activation of SIRT5, a correlation analysis between the IC50 of MC3138 and SIRT5 protein levels was performed. The IC50 value of MC3138 positively correlated with SIRT5 protein

Figure 6. SIRT5 inhibits GOT1 enzymatic activity by catalyzing its lysine deacetylation. (*A*) The lysine acetylation, glutarylation, succinylation, and malonylation levels of GOT1 protein immunoprecipitated from control and *SIRT5*-overexpressing PDAC cells. Inputs are shown below. (*B*) The lysine acetylation level of GOT1 protein immunoprecipitated from control and *SIRT5*-knockdown T3M4/Capan2 cells. Inputs are shown below. (*C*) The lysine acetylation level of GOT1 protein immunoprecipitated from PDAC cells transfected with vector, SIRT5, and mutant SIRT5-H158Y plasmid. Inputs are shown below. (*D*) Exogenous GOT1 protein immunoprecipitated from control and *SIRT5*-knockdown T3M4 cells was subjected to proteomic analysis. *Top*, schematic representation of 3 acetylation sites identified in GOT1; *bottom*, the mass spectrometric signal intensity of indicated acetylation sites in GOT1. (*E–F*) Wild-type *GOT1*, *GOT1-K276R*, *GOT1-K290R*, and *GOT1-K369R* mutant plasmids were transfected into control and *SIRT5*-knockdown T3M4 cells. The lysine acetylation levels of GOT1 protein immunoprecipitated from above cells; inputs are shown below (*E*). The quantification of relative lysine acetylation level of indicated acetylation sites (*F*). (*G–H*) The immunoblotting of SIRT5 and GOT1 levels in scrambled control cells, *SIRT5*-knockdown cells, and *SIRT5*-knockdown/*GOT1*-knockout cells transfected with vector, *GOT1*, or *GOT1-K369R* plasmid. (*I*) The GOT enzyme activity in scrambled control cells, *SIRT5*-knockdown cells, and *SIRT5*-knockdown/*GOT1*-knockout cells transfected with vector, GOT1, or GOT1-K369R plasmids. (*J–K*) Cell growth analysis of scrambled control cells, *SIRT5*-knockdown cells, and *SIRT5*-knockdown/*GOT1*-knockout cells transfected with vector, GOT1, or GOT1-K369R plasmids, cultured under low-glucose conditions (1.25 mmol/L). (*L*) Kinetic flux analysis of ^{13}C-labeled glutamine carbon incorporation into downstream metabolites in scrambled control cells, *SIRT5*-knockdown cells, or *SIRT5*-knockdown/*GOT1*-knockout cells transfected with vector, wild-type *GOT1*, or *GOT1-K369R* plasmids. For all in vitro studies, N $\geq$ 3. The data are represented as mean $\pm$ SD. Student t-test (*D, F*), 1-way ANOVA with Tukey test (*I–K*), 2-way ANOVA with Tukey test (*L*), **P* < .05, ***P* < .01, and ****P* < .001.

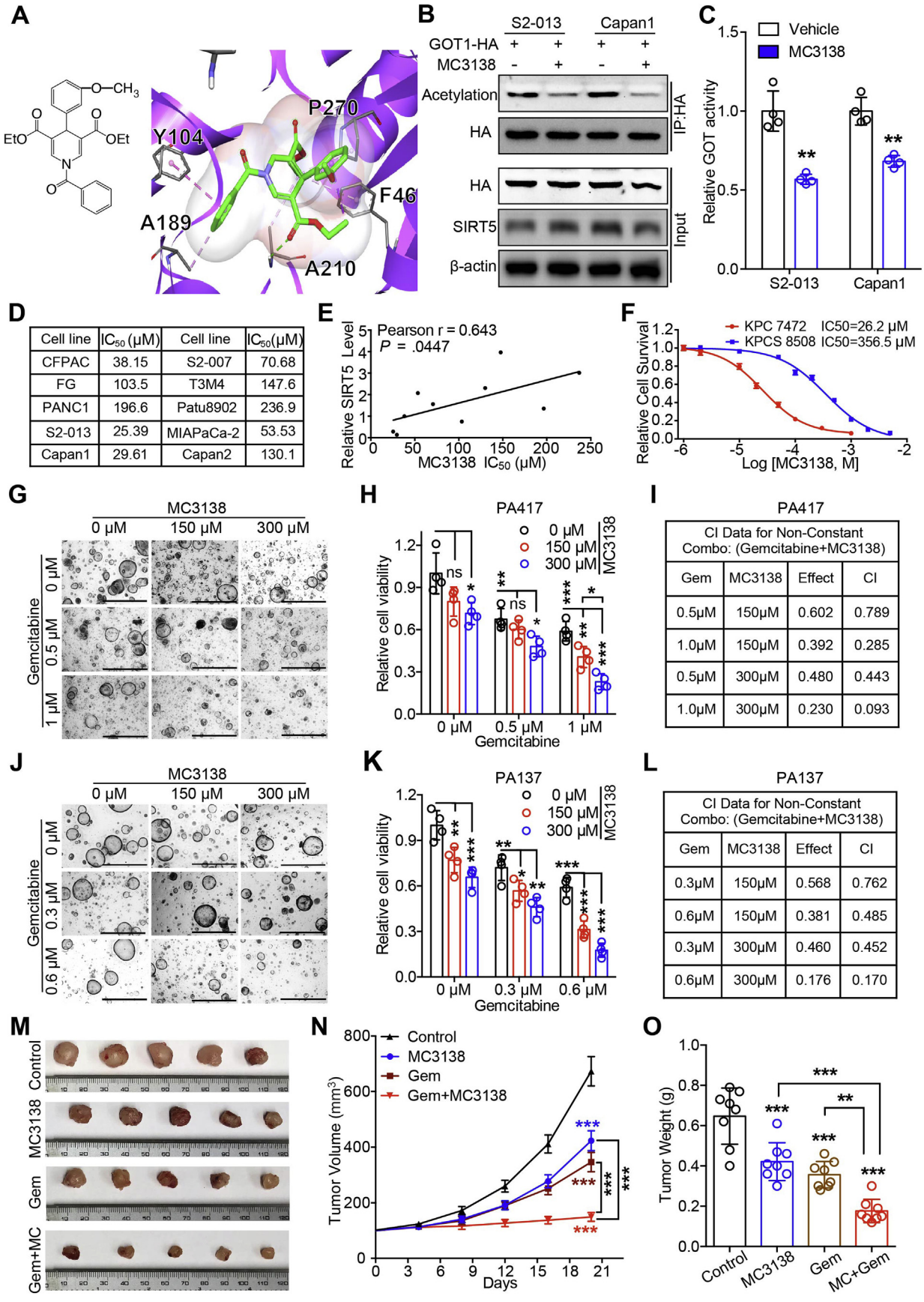

Cell line	IC_{50} (μM)	Cell line	IC_{50}(μM)
CFPAC	38.15	S2-007	70.68
FG	103.5	T3M4	147.6
PANC1	196.6	Patu8902	236.9
S2-013	25.39	MIAPaCa-2	53.53
Capan1	29.61	Capan2	130.1

PA417

CI Data for Non-Constant Combo: (Gemcitabine+MC3138)			
Gem	MC3138	Effect	CI
0.5μM	150μM	0.602	0.789
1.0μM	150μM	0.392	0.285
0.5μM	300μM	0.480	0.443
1.0μM	300μM	0.230	0.093

PA137

CI Data for Non-Constant Combo: (Gemcitabine+MC3138)			
Gem	MC3138	Effect	CI
0.3μM	150μM	0.568	0.762
0.6μM	150μM	0.381	0.485
0.3μM	300μM	0.460	0.452
0.6μM	300μM	0.176	0.170

levels (Figure 7*E*). Moreover, MC3138 was tested in mouse KPC and KPCS cells. Because KPCS cells do not express SIRT5, these cells were, as expected, resistant to MC3138 treatment (Figure 7*F*). Conversely, the SIRT1 activator SRT2104 and SIRT3 activator Honokiol did not exhibit selective growth inhibition between KPC and KPCS cells (Supplementary Figure 8*G–H*). Because *SIRT5* knockdown significantly increased the metabolite levels in glutamine, glutathione, and pyrimidine metabolism pathways (Figure 4*E–H*), these metabolites levels were also investigated in PDAC cells treated using MC3138. MC3138 treatment decreased the metabolite levels in these pathways (Supplementary Figure 8*I–L*). Our previous studies identified that the increase of endogenous pyrimidine pools can diminish the therapeutic efficiency of pyrimidine analog gemcitabine by molecular competition.[30] Next, the combinational effect of MC3138 and gemcitabine, a first-line Food and Drug Administration–approved chemotherapeutic to treat patients with PDAC, was investigated. A combination of gemcitabine and MC3138 at different dosages exhibited synergistic effects in CFPAC-1 and Colo357/FG cells (Supplementary Figure 8*M–P*). Likewise, gemcitabine combined with MC3138 was synergistic at different concentrations in human PDAC organoids with low-SIRT5 expression (Figure 7*G–L*). The MC3138 pharmacokinetics showed that the maximum concentration and half-life of MC3138 in plasma was around 230 μmol/L and 5.059 hours, respectively (Supplementary Figure 8*Q*). To further investigate the effect of gemcitabine combined with MC3138 in vivo, PDX tumors (PA137) were orthotopically implanted in NOD-SCID mice. The concentration of MC3138 in the MC3138-treated tumors ranged from around 100–200 μmol/L, with the average as 143.57 μmol/L, indicating that MC3138 was efficiently delivered to the tumor tissues (Supplementary Figure 8*R*). The combination of gemcitabine and MC3138 significantly decreased tumor size, tumor weight, and tumor proliferation cell index in mice (Figure 7*M–O*, Supplementary Figure 8*S–T*). In addition, the GOT activity was significantly decreased in the MC3138-treated tumors (Supplementary Figure 8*U*). More importantly, the administered drug combination was well tolerated in mice because no significant alterations were observed in body weight and blood biochemistry indices (Supplementary Figure 8*V–W*). Collectively, these data indicate that gemcitabine combined with SIRT5 activator MC3138 can be a potential therapeutic option for PDAC with low-SIRT5 expression.

Discussion

In this work, we established a novel tumor suppressor function of SIRT5 in PDAC cell lines, organoids, orthotopic and spontaneous models, and patients. *SIRT5* knockdown increased PDAC cell growth in normal and nutrient-limited conditions, whereas *SIRT5* overexpression diminished PDAC cell growth. Genetic ablation of *Sirt5* in the mouse spontaneous tumor progression model accelerated acinar-to-ductal metaplasia, PanIN formation, and pancreatic tumorigenesis, which results in decreased survival.

Previous studies demonstrate that *Kras*-mutated PDAC can reprogram its metabolism to adapt to the harsh microenvironment.[5] However, the molecular regulators downstream of oncogenic *Kras* that mediate metabolic adaptations remain poorly characterized. Our present study shows *Sirt5* mRNA and protein levels are decreased in KPC tumor tissues. In the genetically engineered mouse model with the oncogenic $Kras^{G12D}$ mutation, *Sirt5* ablation accelerated PanIN formation and PDAC progression. Hence, *Sirt5* loss potentially functions downstream of *Kras*, and facilitates the oncogenic *Kras* mutation-driven PDAC initiation and development.

Previous studies reveal oncogenic *Kras* mutation-driven PDAC cells use glutamine in a noncanonic way via the GOT2-GOT1-ME1 pathway.[5,31] However, the mechanistic basis of Kras-mediated induction of the pathway is not fully understood. Accordingly, our present study shows that SIRT5 can suppress PDAC progression by inhibiting the GOT1-mediated glutamine/glutathione metabolic pathway via post-translational modification of GOT1. Notably, *SIRT5* knockdown sensitizes PDAC cells to the GOT-inhibitor AOA both in vitro and in vivo. Although the GOT-inhibitor AOA is a pan-aminotransferase inhibitor,[32,33] *SIRT5*-knockdown PDAC cells with significantly higher GOT1 activity were much more sensitive to AOA treatment both in vitro and in vivo (Figure 5*B–G*). Combined with increased glutamine uptake of *SIRT5* knockdown cells, these results indicate SIRT5-mediated deacetylation of GOT1 as a metabolic switch that must be inactivated to facilitate Kras-induced glutamine addiction. Notably, very few studies have

Figure 7. SIRT5 activator MC3138 exhibits antitumor effects and synergism with gemcitabine in human PDAC cells, organoids, and PDX models. (*A*) The chemical structure of SIRT5 activator MC3138 and an enlarged view of SIRT5 docked with MC3138. Protein is shown in purple flat ribbon and compound is depicted via a stick model. (*B*) The lysine acetylation level of GOT1 protein immunoprecipitated from PDAC cells treated with dimethyl sulfoxide (DMSO) or 10 μmol/L MC3138 for 24 h. Inputs are shown below. (*C*) The GOT enzyme activity in PDAC cells treated with DMSO or 10 μmol/L MC3138 for 24 h. (*D*) IC50 data of 10 wild-type PDAC cell lines treated using MC3138. (*E*) Pearson correlation analysis between SIRT5 protein level (from Supplementary Figure 1*L*) and IC50 of MC3138 in PDAC cell lines. (F) Relative cell survival of KPC cell and *SIRT5*-knockout KPC cell (KPCS) treated with MC3138. (*G–H*, *J–K*) Representative images and cell viability of PDAC organoids PA417 (*G–H*) and PA137 (*J–K*) treated with indicated concentration of gemcitabine and MC3138 for 72 h. (*I, L*) Combination index (CI) of gemcitabine and MC3138 at indicated concentrations. "Effect" in the Table refers to the relative cell survival on the combination therapy treatment. (*M–O*) Effect of MC3138 in combination with gemcitabine on PDX (PA137) model. Representative tumor images on necropsy (*M*). Tumor volumes are represented as mean ± SEM (N). Tumor weight on necropsy (O). Gem, gemcitabine; MC, MC3138. For all in vitro studies, N $\geq$ 3. The data are represented as mean ± SD. Student *t* test (*C*), 1-way ANOVA with Tukey test (*H, K, O*), 2-way ANOVA with Tukey test (N), $^{*}P < .05$, $^{**}P < .01$, and $^{***}P < .001$.

reported direct regulation of glutamine metabolism in cancer cells via post-translational modifications that provide nutritional flexibility. Yang et al[34] showed that SIRT3 regulated the malate-aspartate shuttle activity by deacetylating GOT2 in pancreatic cancer. However, unlike GOT1, *GOT2* knockdown could not abolish *SIRT5* knockdown-induced increased cell growth under low-glucose conditions. Two other SIRT5-mediated post-translational modifications have been reported to target glutamine metabolism via SIRT5-mediated desuccinylation of GLS in breast cancer and deglutarylation of GLUD1 in colorectal cancer that increased glutamine uptake and metabolism to support proliferation in other tumor models.[13,16] Conversely, we report increased glutamine uptake and enhanced cell growth in PDAC upon *SIRT5* knockdown. Of note, in a previous study, *GLUD1* knockdown failed to diminish Kras-induced PDAC cell growth; however, *GOT1* knockdown significantly inhibited tumor cell growth.[5] These studies are further supported by our findings and lead to the notion that the mechanistic regulation of glutamine metabolism is distinct in Kras-driven PDAC tumors as compared with tumors of other origin and noncancer cells that are dependent on the canonic glutamine metabolism. Thus, our study demonstrates the mechanistic regulation of noncanonic glutamine metabolism via post-translational modifications in PDAC cells with activating *KRAS* mutations.

Our current study provides the first evidence in support of SIRT5 activation as a therapeutic strategy. We developed a novel first-in-class small-molecule SIRT5 activator, MC3138, which shows selectivity over SIRT1 and SIRT3. Furthermore, MC3138 synergized with gemcitabine in human PDAC cell lines, organoids, and PDX tumors with low-SIRT5 expression. A SIRT5 loss-mediated increase in pyrimidine nucleotide pools provides a potential mechanistic basis for the synergistic effect of the combination with gemcitabine. These results are in line with previous studies demonstrating that molecular competition with increased endogenous pyrimidine pools can outcompete pyrimidine analog gemcitabine and impart resistance.[30] Of note, the toxicity assays indicated MC3138 combined with gemcitabine was well tolerated in mice. These results demonstrate that MC3138 combined with gemcitabine can be a safe and effective therapeutic option for PDAC with low-SIRT5 expression.

In conclusion, our study identifies a vital role SIRT5 plays in regulating glutamine/glutathione metabolism during the initiation and progression of PDAC. Moreover, our data indicate a synergistic effect of the small-molecule SIRT5-activator MC3138 combined with gemcitabine in human PDAC organoids and PDX models. As such, these findings shed new light on the potential use of SIRT5 activation as a novel therapeutic strategy for patients with PDAC with decreased SIRT5 expression.

Supplementary Material

Note: To access the supplementary figures and tables accompany this article, visit the online version of *Gastroenterology* at www.gastrojournal.org, and at http://doi.org/10.1053/j.gastro.2021.06.045.

References

1. Derle A, De Santis MC, Gozzelino L, et al. The role of metabolic adaptation to nutrient stress in pancreatic cancer. Cell Stress 2018;2:332–339.
2. Vernucci E, Abrego J, Gunda V, et al. Metabolic alterations in pancreatic cancer progression. Cancers (Basel) 2019;12.
3. Chaika NV, Yu F, Purohit V, et al. Differential expression of metabolic genes in tumor and stromal components of primary and metastatic loci in pancreatic adenocarcinoma. PLoS One 2012;7:e32996.
4. **Gebregiworgis T, Purohit V**, Shukla SK, et al. Glucose limitation alters glutamine metabolism in MUC1-overexpressing pancreatic cancer cells. J Proteome Res 2017;16:3536–3546.
5. **Son J, Lyssiotis CA**, Ying H, et al. Glutamine supports pancreatic cancer growth through a KRAS-regulated metabolic pathway. Nature 2013;496:101–105.
6. Li M, Chiang YL, Lyssiotis CA, et al. Non-oncogene addiction to SIRT3 plays a critical role in lymphomagenesis. Cancer Cell 2019;35:916–931.e9.
7. Winnik S, Auwerx J, Sinclair DA, et al. Protective effects of sirtuins in cardiovascular diseases: from bench to bedside. Eur Heart J 2015;36:3404–3412.
8. Chalkiadaki A, Guarente L. The multifaceted functions of sirtuins in cancer. Nat Rev Cancer 2015;15:608–624.
9. **Matsushita N, Yonashiro R**, Ogata Y, et al. Distinct regulation of mitochondrial localization and stability of two human Sirt5 isoforms. Genes Cells 2011;16:190–202.
10. Park J, Chen Y, Tishkoff DX, et al. SIRT5-mediated lysine desuccinylation impacts diverse metabolic pathways. Mol Cell 2013;50:919–930.
11. **Nishida Y, Rardin MJ**, Carrico C, et al. SIRT5 regulates both cytosolic and mitochondrial protein malonylation with glycolysis as a major target. Mol Cell 2015;59:321–332.
12. Yang X, Wang Z, Li X, et al. SHMT2 desuccinylation by SIRT5 drives cancer cell proliferation. Cancer Res 2018;78:372–386.
13. Wang YQ, Wang HL, Xu J, et al. Sirtuin5 contributes to colorectal carcinogenesis by enhancing glutaminolysis in a deglutarylation-dependent manner. Nat Commun 2018;9:545.
14. **Li F, He X, Ye D**, et al. NADP(+)-IDH mutations promote hypersuccinylation that impairs mitochondria respiration and induces apoptosis resistance. Mol Cell 2015;60:661–675.
15. Chen XF, Tian MX, Sun RQ, et al. SIRT5 inhibits peroxisomal ACOX1 to prevent oxidative damage and is downregulated in liver cancer. EMBO Rep 2018;19:e45124.
16. **Greene KS, Lukey MJ**, Wang X, et al. SIRT5 stabilizes mitochondrial glutaminase and supports breast cancer tumorigenesis. Proc Natl Acad Sci U S A 2019;116:26625–26632.
17. Yan D, Franzini A, Pomicter AD, et al. Sirt5 is a druggable metabolic vulnerability in acute myeloid leukemia. Blood Cancer Discov 2021;2:266–287.

18. **Giblin W, Bringman-Rodenbarger L, Guo AH**, et al. The deacylase SIRT5 supports melanoma viability by influencing chromatin dynamics. J Clin Invest 2021; 131:e138926.
19. **Abril YLN, Fernandez IR**, Hong JY, et al. Pharmacological and genetic perturbation establish SIRT5 as a promising target in breast cancer. Oncogene 2021; 40:1644–1658.
20. Hingorani SR, Petricoin EF, Maitra A, et al. Preinvasive and invasive ductal pancreatic cancer and its early detection in the mouse. Cancer Cell 2003; 4:437–450.
21. **Olive KP, Tuveson DA**, Ruhe ZC, et al. Mutant p53 gain of function in two mouse models of Li-Fraumeni syndrome. Cell 2004;119:847–860.
22. **Du J, Zhou Y, Su X**, et al. Sirt5 is a NAD-dependent protein lysine demalonylase and desuccinylase. Science 2011;334:806–809.
23. Dasgupta A, Shukla SK, Vernucci E, et al. SIRT1-NOX4 signaling axis regulates cancer cachexia. J Exp Med 2020;217:e20190745.
24. Strobel O, Dor Y, Alsina J, et al. In vivo lineage tracing defines the role of acinar-to-ductal transdifferentiation in inflammatory ductal metaplasia. Gastroenterology 2007; 133:1999–2009.
25. Nakagawa T, Lomb DJ, Haigis MC, et al. SIRT5 Deacetylates carbamoyl phosphate synthetase 1 and regulates the urea cycle. Cell 2009;137:560–570.
26. **Rardin MJ, He W**, Nishida Y, et al. SIRT5 regulates the mitochondrial lysine succinylome and metabolic networks. Cell Metab 2013;18:920–933.
27. Sadhukhan S, Liu X, Ryu D, et al. Metabolomics-assisted proteomics identifies succinylation and SIRT5 as important regulators of cardiac function. Proc Natl Acad Sci U S A 2016;113:4320–4325.
28. **Zhou L, Wang F**, Sun R, et al. SIRT5 promotes IDH2 desuccinylation and G6PD deglutarylation to enhance cellular antioxidant defense. EMBO Rep 2016;17:811–822.
29. Schwer B, Bunkenborg J, Verdin RO, et al. Reversible lysine acetylation controls the activity of the mitochondrial enzyme acetyl-CoA synthetase 2. Proc Natl Acad Sci U S A 2006;103:10224–10229.
30. **Shukla SK, Purohit V, Mehla K**, et al. MUC1 and HIF-1alpha signaling crosstalk induces anabolic glucose metabolism to impart gemcitabine resistance to pancreatic cancer. Cancer Cell 2017;32:71–87.e7.
31. Abrego J, Gunda V, Vernucci E, et al. GOT1-mediated anaplerotic glutamine metabolism regulates chronic acidosis stress in pancreatic cancer cells. Cancer Lett 2017;400:37–46.
32. Korangath P, Teo WW, Sadik H, et al. Targeting glutamine metabolism in breast cancer with aminooxyacetate. Clin Cancer Res 2015;21:3263–3273.
33. Hao Y, Samuels Y, Li Q, et al. Oncogenic PIK3CA mutations reprogram glutamine metabolism in colorectal cancer. Nat Commun 2016;7:11971.
34. **Yang H, Zhou L**, Shi Q, et al. SIRT3-dependent GOT2 acetylation status affects the malate-aspartate NADH shuttle activity and pancreatic tumor growth. EMBO J 2015;34:1110–1125.

Author names in bold designate shared co-first authorship.

Received January 21, 2021. Accepted June 13, 2021.

Correspondence
Address correspondence to: Pankaj K. Singh, PhD, Eppley Institute for Research in Cancer and Allied Diseases, University of Nebraska Medical Center, 987696 Nebraska Medical Center, Omaha, Nebraska 68198-7696. e-mail: Pankaj.singh@unmc.edu.

CRediT Authorship Contributions
Tuo Hu, PhD (Conceptualization: Lead; Investigation: Lead; Writing – original draft: Equal).
Surendra Shukla, PhD (Investigation: Supporting; Resources: Supporting; Writing – review & editing: Supporting).
Enza Vernucci, PhD (Conceptualization: Supporting; Formal analysis: Supporting; Investigation: Supporting; Writing – review & editing: Supporting).
Chunbo He, BS (Investigation: Supporting).
Dezhen Wang, PhD (Investigation: Supporting).
Ryan King, PhD (Investigation: Supporting).
Kanupriya Jha, MS (Investigation: Supporting; Visualization: Supporting).
Kasturi Siddhanta, MS (Formal analysis: Supporting; Investigation: Supporting).
Nicholas Mullen, BS (Investigation: Supporting; Writing – review & editing: Supporting).
Kuldeep Attri, PhD (Investigation: Supporting).
Divya Murthy, PhD (Investigation: Supporting).
Nina Chaika, MS (Investigation: Supporting).
Ravi Thakur, PhD (Investigation: Supporting).
Scott Mulder, PhD (Investigation: Supporting).
Camila Pacheco, BS (Methodology: Supporting).
Xiao Fu, PhD (Investigation: Supporting).
Robin Fu, MA (Formal analysis: Supporting).
Fang Yu, PhD (Formal analysis: Lead).
Audrey Lazenby, MD (Formal analysis: Supporting; Methodology: Supporting).
Clemens Steegborn, PhD (Investigation: Supporting).
Ping Lan, PhD (Resources: Supporting).
Kamiya Mehla, PhD (Investigation: Supporting; Methodology: Supporting).
Dante Rotili, PhD (Investigation: Supporting).
Sergio Valente, PhD (Resources: Supporting).
Sarika Chaudhary, PhD (Data curation: Supporting; Supervision: Supporting).
Marco Tafani, PhD (Resources: Supporting).
Antonello Mai, PhD (Resources: Supporting; Supervision: Supporting).
Johan Auwerx, PhD (Resources: Supporting).
Eric Verdin, PhD (Resources: Supporting).
David Tuveson, PhD (Resources: Supporting).
Pankaj Singh, PhD (Conceptualization: Lead; Funding acquisition: Lead; Supervision: Lead; Writing – original draft: Supporting; Writing – review & editing: Lead).

Conflicts of interest
The authors disclose no conflicts.

Funding
This work was supported in part by the funding from National Institutes of Health (R01 CA216853, R01CA210439, R01CA163649, and P01 CA2117798, National Cancer Institute [NCI]) to Pankaj K. Singh, (Specialized Programs of Research Excellence [SPORE], 2P50 CA127297, NCI) to Pankaj K. Singh, the Italian Association for Cancer Research (AIRC) 2016 (number 19162) to Antonello Mai, and (P30 CA036727, NCI) for supporting shared resources. A part of Tuo Hu's stipend was supported by the China Scholarship Council program; they had no role in the study design in the collection, analysis, and interpretation of data.